LIMNOLOGY
and
OCEANOGRAPHY

ASLO

Limnol. Oceanogr. 00, 2020, 1–21

doi: 10.1002/lno.11404

Interactive effects of iron and light limitation on the molecular physiology of the Southern Ocean diatom *Fragilariopsis kerguelensis*

Carly M. Moreno,[1] **Weida Gong**,[1] **Natalie R. Cohen**,[1,2] **Kimberly DeLong**,[1,3] **Adrian Marchetti**[1*]

[1]Department of Marine Sciences, University of North Carolina at Chapel Hill, Chapel Hill, North Carolina
[2]Marine Chemistry and Geochemistry Department, Woods Hole Oceanographic Institution, Woods Hole, Massachusetts
[3]Ocean Sciences Department, University of California, Santa Cruz, Santa Cruz, California

Abstract

The polar diatom *Fragilariopsis kerguelensis* is ubiquitous in Southern Ocean waters and is a major responder to iron fertilization, encountering large gradients in iron concentrations and light availability. We performed a comparative transcriptomic analysis of *F. kerguelensis* grown under varying iron and light conditions in order to investigate the molecular underpinnings that may explain its physiological response to iron and light limitation. Low iron reduced growth rates more than low light, but there was not an additive effect of low iron and low light on growth rate. Low iron treatments (saturating and low light) had the largest transcriptomic response; however, expression patterns were more similar in low light treatments (high and low iron). Under iron and light limitation, carbon fixation and amino acid, ribosome, and sulfur metabolisms were overrepresented relative to the control (iron replete, saturating light). Transcripts of genes encoding for the proteins aquaporin, proteorhodopsin, plastocyanin, and flavodoxin were overrepresented to the greatest extent in the low iron/low light treatment, indicating there may be an additive effect of iron/light colimitation at the molecular level. Iron and light replete cells demonstrated increased expression of genes encoding for the proteins ferritin, carbonic anhydrase, and numerous iron-dependent proteins relative to the growth-limiting treatments. This transcriptome analysis reveals mechanisms that may underpin the ecological success of this diatom in low iron and light environments, highlighting the important role of diversified photosynthetic isoforms, iron acquisition, unique detoxification mechanisms of reactive oxygen species, and metabolic shifts in amino acid recycling and carbon metabolism.

The Southern Ocean (SO) has a disproportionately large influence on global biogeochemical cycles by transporting and storing nutrients, heat, and anthropogenic CO_2 (Sarmiento et al. 2004; Gruber et al. 2009). Biological processes in the SO are mediated by phytoplankton, of which diatoms can be responsible for as much as 75% of annual primary production (Tréguer et al. 1995) and almost all of the silica sedimentation below the Antarctic Circumpolar Current (ACC) (Abelmann et al. 2006; Tréguer et al. 2014). Furthermore, nutrient inventories in the low latitudes, where water upwells after being subducted in the SO, are largely determined by SO diatom productivity and subsequent nutrient utilization (Sarmiento et al. 2004; Assmy et al. 2013). Diatoms in this region support massive krill stocks that sustain a diverse and rich marine food web of fish, birds, seals, and whales (Saba et al. 2014).

SO diatoms must cope with extreme environmental conditions characterized by steep gradients in chemical and physical properties such as iron and light availability. The SO is the largest high nutrient, low chlorophyll (HNLC) region in which nitrate concentrations are consistently high and phytoplankton productivity is limited by the availability of the micronutrient iron (Martin 1990; Boyd et al. 2007). New iron inputs are episodic, primarily from aeolian dust deposition, glacial meltwater discharge, resuspension of sediments, and deep winter mixing; however, rapid biological uptake and particle scavenging quickly deplete available iron in the upper ocean (Edwards and Sedwick 2001; Cassar et al. 2007). Investigations of artificial and natural iron fertilization experiments have shown that upon iron enrichment, the growth rates of large diatoms increase and they soon comprise the bulk of the phytoplankton biomass (de Baar et al. 1990; Arrigo et al. 1998; Boyd et al. 2000; Blain et al. 2007). However, when iron concentrations are low, diatoms must be able to survive until another pulse of iron becomes available.

Iron is used in many enzymes within the cell and is particularly abundant in proteins involved in photosynthesis (Raven 2013). Iron limitation results in the reduction of diatom growth rate, photosynthetic efficiency, and chlorophyll *a* (Chl *a*) content (Sunda and Huntsman 1995; Timmermans et al. 2001;

*Correspondence: amarchetti@unc.edu

Additional Supporting Information may be found in the online version of this article.

Arrigo et al. 2010). To cope with iron limitation, diatoms invoke a number of acclimation strategies that include substitutions of iron-containing proteins with non-iron equivalents (La Roche et al. 1996; Maldonado et al. 2006; Peers and Price 2006), a reduction in cell size, reduction in iron to carbon ratio (Sunda and Huntsman 1995; Strzepek and Harrison 2004), luxury uptake of iron (Marchetti et al. 2009), altering photosynthetic architecture (Strzepek et al. 2012), and in some diatoms, induction of a high affinity iron uptake system (Kustka et al. 2007; Lommer et al. 2012; McQuaid et al. 2018).

In addition to large gradients in iron availability, diatoms must cope with variations in light availability. Daily and seasonal variations in irradiance are extreme at high latitudes and deep mixing by strong winds results in low average light intensities within the mixed layer (Boyd et al. 2001). Diatoms that overwinter in the SO can experience considerable periods of light limitation (Sallée et al. 2010). During austral summer, light limitation may still persist due to deep mixed layers and diatoms may not benefit from iron inputs if wind-driven mixing dominates over the effects of stratification (Mitchell et al. 1991; van Oijen 2004). Thus, there is high potential for iron and light colimitation in SO diatoms throughout the growing season (Boyd 2002; Galbraith et al. 2010; Cassar et al. 2011). Polar diatoms may also increase the size, rather than the number, of their photosynthetic subunits under low light, thereby minimizing their overall iron requirements (Strzepek et al. 2012). Yet the specific molecular underpinnings of acclimation to low light by iron-limited diatoms remain largely unknown.

Fragilariopsis, a genus of pennate diatoms, are among the most dominant diatoms in the pelagic zone and in sea ice of polar regions (Boyd et al. 2000; Hoffmann et al. 2007; Strzepek et al. 2011). Frustules of *F. kerguelensis* are particularly robust (Hamm et al. 2003) and have been proposed to serve as proxies for paleoceanographic processes as their frustules comprise as much as 70% of the marine biogenic silica in sediments below SO current systems (Zielinski and Gersonde 1997; Assmy et al. 2006; Marchetti and Cassar 2009; Tréguer et al. 2014). Numerous studies have demonstrated that *F. kerguelensis* has adapted to residing in iron deprived waters of the ACC by reducing cellular iron demands and accessing a wide range of iron forms (Timmermans et al. 2004; Assmy et al. 2006; Timmermans and van der Wagt 2010; Strzepek et al. 2011). *F. kerguelensis* is a main responder to artificial iron enrichment experiments and is abundant in naturally iron-fertilized waters (Boyd et al. 2000; Blain et al. 2007; Hoffmann et al. 2007). Its frustules are heavily silicified and can deplete surface waters of silicic acid to a greater extent than nitrate, thereby decoupling silicon and carbon cycles in the SO and reducing silicic acid concentrations in subducted waters that are eventually transported to lower latitude regions (Sarmiento et al. 2004; Assmy et al. 2013).

Interacting environmental factors influence phytoplankton assemblages in the SO. While several studies have examined the physiological responses of SO diatoms to the interactive effects of iron and light, as well as other factors such as temperature and CO_2 (van Oijen 2004; Feng et al. 2010; Hoppe et al. 2013; Boyd et al. 2015), few have investigated the molecular underpinnings orchestrating these physiological responses to individual or interactive effects (Mock et al. 2017). Several laboratory and field-based studies have investigated the growth and physiology of *F. kerguelensis*, as well as other species of this genus, in relation to the interactive effects of iron and light limitation (Timmermans et al. 2004; Hoffmann et al. 2007; Timmermans and van der Wagt 2010); however, molecular explanations were not provided. An understanding of species-specific physiological and molecular responses to these commonly limiting growth variables is necessary given the importance of diatoms to ocean biogeochemical cycles.

Here, we examined an isolate of *F. kerguelensis* exposed to a matrix of light and iron levels in order to investigate both independent and interactive effects of limitation on its transcriptome and inferred physiology. Using *de novo* transcriptome assemblies sequenced as part of the Marine Microbial Expressed Transcriptome Sequencing Project (MMETSP) (Keeling et al. 2014), we performed a comparative gene expression analysis to investigate the response of *F. kerguelensis* to steady-state iron and light limitation. Gene expression patterns obtained through comparative transcriptome analyses were confirmed through quantitative reverse transcriptase polymerase chain reaction (RT-qPCR) for select target genes. In particular, we investigated pathways that are predicted to be significantly affected by iron and/or light limitation, such as photosynthesis, nitrogen assimilation, carbon metabolism, and iron homeostasis. By leveraging high-throughput sequencing of *F. kerguelensis* mRNA, we have gained a more complete understanding of the molecular processes underpinning this diatom's unique physiological characteristics.

Materials and methods

Culture conditions and growth characteristics

Experiments were performed with *Fragilariopsis kerguelensis* strain L26-C5, isolated from the Atlantic Sector of the SO (48°S, 16°W) in 2009 (18S GenBank accession number KJ866919). Cells were maintained at 4°C, under a continuous photon flux density of either 10 μmol photons m^{-2} s^{-1} (low light [LL]) or 90 μmol photons m^{-2} s^{-1} (growth saturating light [SL]) until the variation in specific growth rates between transfers did not exceed 10% (4–5 cell transfers). Cells were grown in standard AQUIL medium using trace metal clean techniques (Marchetti et al. 2006). Macronutrients were added to achieve final concentrations of 300 μmol L^{-1} NO_3, 200 μmol L^{-1} $Si(OH)_4$, and 20 μmol L^{-1} PO_4. Vitamins (cyanocobalamin, thiamine, and biotin) and trace metals were filter-sterilized through 0.2 μm cutoff Acrodiscs before being added to the medium. Trace metals were buffered using 100 μmol L^{-1} of EDTA according to Price et al. (1989). Iron-replete treatments (+Fe) were prepared by adding 1370 nmol L^{-1} of total

iron (FeT) in a 1:1 Fe:EDTA solution to Aquil medium, corresponding to a dissolved inorganic iron (Fe′) concentration of 2.7 nmol L^{-1}. Iron-limited treatments (−Fe) were prepared by adding 3.1 nmol L^{-1} FeT to achieve an Fe′ concentration of 6 pmol L^{-1} (Marchetti et al. 2009). Cultures were grown in acid-washed 28 mL polycarbonate centrifuge tubes (Nalgene) and maintained in exponential phase by serial transfer. Specific growth rates of cells between transfers were calculated from the linear regression of the natural log of *in vivo* Chl *a* fluorescence using a Turner 10-AU fluorometer (Brand et al. 1981).

Photophysiological parameters such as the maximum quantum efficiency of photosystem II (F_v/F_m) were measured with a Fluorescence Induction Relaxation System (FIRe) (Satlantic). Samples were dark acclimated for at least 10 min and triplicate measurements were taken of each culture for F_v/F_m and functional absorption cross-section of PSII (σ_{PSII} [nm^2 $quanta^{-1}$]). The excitation wavelength was 450 nm with other parameters set to measure single turnover flash (80 μs) of PSII reaction centers (single closure event) with a sample delay of 1000 ms (Gorbunov and Falkowski 2005). To test for statistically significant differences in growth rate and photophysiology between treatments, a two-way ANOVA was performed. Data sets were tested for normality and equal variance, and Tukey pairwise multiple comparison tests was performed using SigmaPlot 12.5. The level of significance was $p < 0.05$.

Cultures for high-throughput sequencing of mRNA were grown in acid-washed 2-liter polycarbonate bottles. After reaching late exponential phase, cultures were harvested onto polycarbonate filters (3.0 μm pore size, 25 mm), flash frozen in liquid nitrogen and immediately stored at −80°C. Total RNA was extracted using the RNAqueous 4PCR Kit (Ambion) according to the manufacturer's protocols. Initial bead beating was performed to remove all cells from the filters and lyse cells. Residual genomic DNA was removed by DNAse I digestion at 37°C for 45 min and then purified with DNase inactivation reagent (Ambion).

Sequencing, assembly, read counts, and annotation

Library preparations, sequencing, transcriptome assembly, annotations, and generating read counts were carried out by the MMETSP with the following protocol (Keeling et al. 2014). RNA was quantified with the Invitrogen Qubit Q32855 and the quality was assessed using the Agilent 2100 Bioanalyzer. Libraries were made from approximately 2 μg RNA using Illumina's TruSeq RNA Sample Preparation Kit. The average insert size of each library ranged from 250 to 350 bp. Libraries were sequenced on the Illumina HiSeq 2000 to obtain 2×50 bp (paired-end) reads. Transcriptome assembly was carried out using the internal pipeline BPA2.0 (Batch Parallel Assembly version 2.0) from the National Center of Genome Resources. Sequence reads were preprocessed using the string graph assembler SGA algorithm for quality trimming (swinging average) at Q15 (Simpson and Durbin 2011). Reads less than 25 bp after trimming were discarded. Preprocessed sequence reads from each individual sample were assembled into contigs with ABySS v1.3.3, using 20 unique kmers between $k = 26$ and $k = 50$ (Simpson et al. 2009). ABySS parameters are as follows: minimum kmer coverage of 5, popping at > 0.9 branch identity, with the scaffolding flag disabled to avoid over-reduction of divergent regions. Unitigs from all kmer assemblies and all samples were combined and redundancies were removed using CD-HIT-EST with a clustering threshold identity of 0.98 (Li and Godzik 2006). The overlap layout consensus assembler CAP3 was used to identify minimum 100 bp overlaps between the resultant contigs and assemble larger sequences (Xiaoqui and Anup 1999). The resulting contigs were paired-end scaffolded using ABySS. Sequence read pairing information was used in GapCloser (SOAP *de novo* package v1.10; Luo et al. 2015) to close gaps created during scaffolding. Redundant sequences were again removed using CD-HIT-EST at a clustering threshold of 0.98 identity. The consensus contigs were filtered to a minimum length of 150 bp to produce the final set of contigs.

Read counts were generated with Bowtie 2 v2.2.5 (default parameters) by mapping raw reads from each treatment transcriptome to the contigs of the combined assembly (Langmead and Salzberg 2012). Only unique read pairs that aligned once were reported. Reads were filtered by mapping quality with SAMtools v1.2. BUSCO v2 (Benchmarking Universal Single-Copy Orthologs) software was used to assess the completeness of each transcriptome and the combined assembly (Simão et al. 2015). Coding sequences (CDS) were predicted using ESTScan with a Bacillariophyta scoring matrix (Iseli et al. 1999; Lottaz et al. 2003). Peptide predictions over 30 amino acids in length were annotated. CDS annotation by homology was determined using BLASTx (E-value ≤ 10^{-5}) to the Kyoto Encyclopedia of Genes and Genomes (KEGG, Release 80.2; Kanehisa et al. 2006). Only the top KEGG Ortholog (KO) and module annotation (MO) hits were chosen for further analysis. Read counts for identically annotated functional genes, that is, KOs, were summed together. For pathway level analysis, at the module (MO) and KEGG Class 3 level, read counts corresponding to KOs contained within each MO were also summed together. For genes of interest that do not have a KO, but had a KEGG functional gene definition (e.g., ISIPs, RHO, CREG) read counts corresponding to these definitions were summed.

Differential gene expression

The edgeR v3.12.0 package was used to normalize reads with the trimmed means of M normalization method (TMM) and to detect differentially expressed genes in comparisons between the iron replete, saturating light control (+FeSL) and the tested treatments: iron-limited, saturating light (−FeSL); iron replete, low light (+FeLL); and iron-limited, low light (−FeLL) (Robinson and Smyth 2007; Robinson et al. 2009). We estimated dispersion from a reduced design model by treating similar treatments as replicates (+Fe vs. −Fe and SL vs. LL). Because differences in treatments must be larger than

those in replicates, we estimated a conservative dispersion coefficient of 0.1 subsequently used in the model across all samples to determine significance (p value < 0.05). The exactTest was used to determine normalized fold change (FC) and counts-per-million (CPM). This approach resulted in a relatively small set of significantly differentially expressed genes (DEGs). DEGs that recruited higher or lower normalized transcript abundance in the treatment relative to the control are described as overrepresented or underrepresented, respectively. Gene expression FC was used to visualize treatment-specific differences of gene expression at the KO level. Normalized reads that were assigned to KOs were then grouped together into pathway level modules (MO). A Wilcoxon rank-sum test was used to determine significantly differentially expressed MOs. Finally, KOs that had KEGG Class 3 annotations were grouped together to determine broad level changes in cell metabolism. FCs were used to visualize KO, MO and Class 3 level expression patterns in heatmaps, ratio average plots, and cell schematic figures. CPM was used to visualize ternary figures at all three annotation levels. All figures were generated in R using ggplot2 (Wickham 2016) and ggtern (Hamilton 2018) packages.

qPCR validation of differential gene expression

Primers for genes of interest used for qPCR validation of the transcriptome were designed using Primer3 v0.4.0 (Supporting Information Table SS1). Amplification efficiency of each primer pair was determined by creating a fivefold dilution of template material and plotting cycle threshold values on a logarithmic scale, along with corresponding concentrations, to generate a linear regression curve. Efficiency was calculated using the slope of the curve and the equation $E = -1 + 10^{(-1/\text{slope})}$. Primer efficiencies ranged between 92% and 109%. Correct target primer amplification was determined with Sanger sequencing of the PCR product (Supporting Information Table SS1). Up to 2 μg of cDNA was reverse transcribed with the SuperScript III First-Strand cDNA Synthesis kit with oligo-dT primers (Invitrogen). RT-qPCR was performed on synthesized cDNA with a Mastercycler ep realplex (Eppendorf) and the KAPA SyberFast qPCR kit mix (Kapa). Relative gene expression of 10 genes in relation to the housekeeping genes Actin (*ACT)* and Tubulin (*TUB)* was determined using the Pfaffl method with primer efficiency correction (Pfaffl 2001). Correlation was evaluated using Pearson correlation coefficients.

Results and discussion

Comparative transcriptomics was used to understand how the SO diatom *F. kerguelensis* responds to low iron, low light, and combined low iron/low light conditions. Several investigations have previously reported the gene expression patterns or protein responses of diatoms and other ecological important phytoplankton groups to acclimated iron limitation or rapidly induced iron stress (Lommer et al. 2012; Nunn et al. 2013; Mock et al. 2017; Koch et al. 2019), as well as the metatranscriptomic responses of phytoplankton to iron enrichment in temperate oceans (Marchetti et al. 2012; Cohen et al. 2017*b*) and Antarctic waters (Bertrand et al. 2015; Pearson et al. 2015). However, few studies have investigated the whole transcriptome response of a polar diatom to the interactive effects of iron and light limitation. By leveraging the high-throughput transcriptome sequencing efforts of the MMETSP, we have performed a comparative gene expression analysis of *F. kerguelensis* using *de novo* transcriptomics under three growth-limited conditions relative to an iron replete, saturating light control. We used conservative methods to interpret our data and analyzed transcription patterns of both single genes and overall pathways in order to achieve a higher level of confidence to elucidate the collective transcription patterns in this ecologically important diatom.

Growth characteristics

Numerous laboratory-based experiments, and both artificial and natural iron enrichment studies, have shown that *F. kerguelensis* and other large diatoms are quickly altered in terms of growth rates, nutrient uptake ratios, and morphology following the addition of iron to iron-limited cells (Boyd et al. 2001; Timmermans et al. 2004; Timmermans and van der Wagt 2010). In the present study, iron and/or light limitation influenced growth rates, photophysiology, and the transcriptome of steady-state *F. kerguelensis* cells (Fig. 1A–C). The maximum growth rate in the iron replete, saturating light (+FeSL) control was 0.22 ± 0.01 d^{-1}, consistent with other published studies that ranged from 0.2 to 0.4 d^{-1} (Timmermans et al. 2001; Hoffmann et al. 2007; Timmermans and van der Wagt 2010). Limitation of Fe (−FeSL) or light (+FeLL) reduced growth rates by 70% and 37%, respectively (Fig. 1A; Supporting Information Fig. SS1A). Growth rates were not further reduced in the combined low Fe/low light (−FeLL) treatment compared to the low Fe (−FeSL) treatment, indicating *F. kerguelensis* growth rates do not exhibit an additive effect of iron and light limitation. In other words, iron limitation had a greater effect on growth rate, while light limitation in iron-limited cells may be partially relieved by intracellular mechanisms. As we do not see a statistical difference in growth rates in low iron conditions between light treatments, potential enhancement in Fe′ concentrations produced by the photodissociation of ferric iron chelates do not appear to be sufficient to significantly affect the growth rate in the low Fe (−FeSL), EDTA-buffered cultures (Sunda and Huntsman 1995).

In addition to a reduction in growth rates, iron and/or light limitation affected the photochemical efficiency (F_v/F_m) and the absorption cross-section of PSII (σ_{PSII}). Iron-replete diatoms had comparable, but significantly different F_v/F_m at high and low light, with the maximum F_v/F_m of 0.73 measured under low light (Fig. 1B). Iron-limited cells had reduced F_v/F_m, at both high light (26% reduction) and low light (18% reduction) compared to the control. Iron-replete σ_{PSII} values were comparable,

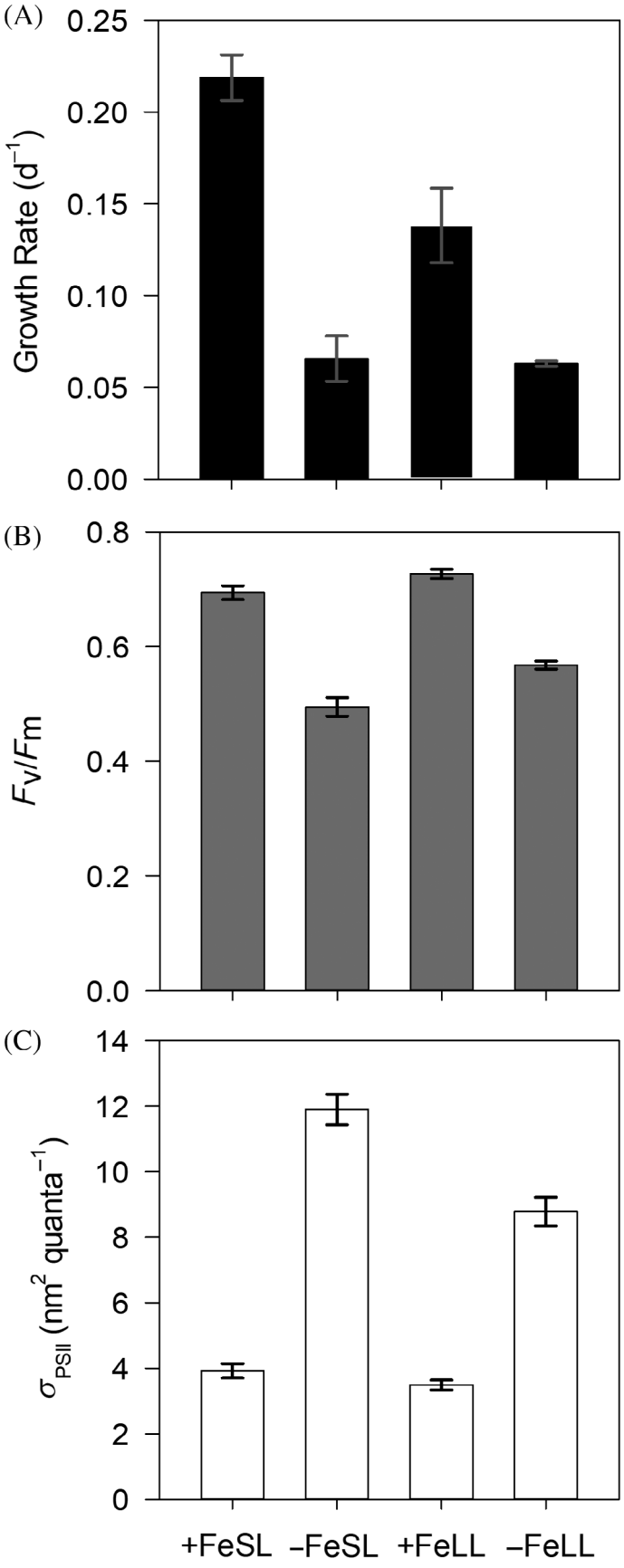

~ 3.7 nm^2 quanta^{-1}, and not significantly different from each other between light treatments (Fig. 1C). Iron limitation increased σ_{PSII} by threefold under saturating light and by twofold under low light. As was expected from previous studies (Suggett et al. 2009; Strzepek et al. 2012), there was an inverse relationship between F_v/F_m and σ_{PSII} among the four treatments (Supporting Information Fig. SS1B); however, in the low Fe/low light (–FeLL) treatment, F_v/F_m was higher and σ_{PSII} was lower than in low Fe (-FeSL), indicating a more efficient photosystem in the former treatment. As diatoms in the ACC are often mixed out of the euphotic zone, it may be beneficial if they maintained the structure of their photosynthetic subunits under low light or darkness whether iron-limited or not, as they could then quickly take advantage of light when they are brought to the surface (Peters and Thomas 1996).

RNA sequencing, assembly, and validation

The transcriptome size and sequencing statistics for *F. kerguelensis* were overall within range of a majority of transcriptomes sequenced within the MMETSP, including number of reads and contigs, N50, mapping efficiency, and BUSCO completeness scores (Keeling et al. 2014). High-throughput sequencing yielded an average of 46 million raw reads for each treatment, resulting in a combined assembly with approximately 184 million raw reads (Table 1). The NCGR assembly pipeline produced approximately 50,000 contigs per treatment, resulting in a combined nonredundant assembly with 75,180 contigs with a range of contig lengths from 500 to 23,605 bp. Transcriptomes corresponding to each treatment were assigned an average BUSCO completion score of ~ 74%, suggesting a comprehensive coverage of functional core genes. Read mapping efficiencies were between 70% and 75%. Approximately 15% of the differentially expressed genes in each transcriptome were associated with KEGG functional annotations. The number of functionally annotated genes detected was 2999 and is equivalent to other MMETSP sequenced diatoms (Bender et al. 2014; Cohen et al. 2017*a*) and prymnesiophytes (Koid et al. 2014). An exploratory, multidimensional scaling plot of KO annotated gene expression profiles of each library revealed that treatments could be distinguished based on replete (+FeSL) or stressed conditions (+FeLL, –FeSL, –FeLL) and that low light treatments (+Fe, –Fe) were more similar to each other than low Fe (SL, LL) (Supporting Information Fig. S2). The transcriptome and RT-qPCR analysis of single genes of interest demonstrated considerable agreement between treatments and the control,

Fig. 1. Growth characteristics of *F. kerguelensis*. (**A**) Specific growth rates, (**B**) maximum photochemical yield of PSII (F_v/F_m), and (**C**) the functional absorption cross-section of PSII (σ_{PSII}; [nm^2 quanta^{-1}]) of *F. kerguelensis* as a function of iron and light status. Treatments are Fe-replete, saturating light (+FeSL; served as control), Fe-limited, saturating light (–FeSL), Fe-replete, light-limited (+FeLL), and Fe-limited, light-limited (–FeLL). Error bars represent the standard deviation of biological triplicates.

Table 1. Sequencing statistics, transcriptome coverage, and mapping statistics.

	+FeSL	−FeSL	+FeLL	−FeLL	Combined assembly
Raw sequence reads	43,124,296	45,553,318	49,019,016	47,136,326	184,832,956
Number of contigs	50,930	56,173	51,006	48,729	75,180
Maximum length (bp)	23,605	16,027	16,160	16,511	16,675
Minimum length (bp)	150	150	150	150	150
N50	1927	1754	1818	1786	1546
BUSCO Eukaryota (%)	74	74	72	75	74
Functionally annotated (%)	13	15	15	15	—
Mapping efficiency to combined assembly (%)	70	73	74	75	—

validating the precision of the RNAseq approach for gene expression analysis ($R = 0.66$, $p < 0.003$) (Supporting Information Fig. S3).

Photosynthetic energy production and photoprotective strategies

The ability of *F. kerguelensis* to survive and often bloom in the SO could be due to its highly adapted photosynthetic capability, particularly under conditions of low iron and light availability. Therefore, we examined transcriptional patterns of genes involved in photosynthesis, light harvesting, and related pathways. Despite poly-A selection for nuclear transcripts, a large number of plastid-related transcripts, many of which are not polyadenylated, were detected in the *F. kerguelensis* transcriptome. These transcripts are useful in understanding changes occurring within the photosynthesis pathway and other chloroplast-related processes (Lima and Smith 2017). Yet expression patterns of genes that do not contain a poly-A tail should be interpreted with caution as their partial removal implies they may no longer be proportionally represented. Furthermore, many of the genes and metabolic pathways identified as having large expression changes under low iron and/or low light conditions inherently include metabolic shifts that could also naturally occur under any growth limitation; therefore, it may be difficult to tease apart the specific effects of low iron and/or low light compared to that of a general effect of decreased growth on the expression of certain genes and metabolic pathways.

As expected, the broad photosynthesis metabolic pathway was consistently underrepresented in all treatments compared to the control (Figs. 2, 3A); however, at the individual photosystem and subunit levels, there were contrasting expression patterns (Figs. 3B, 4). Despite both photosystems requiring iron (PSII requires two iron atoms per subunit while PSI requires 12 atoms per subunit) (Strzepek et al. 2012), PSI was overrepresented 4.6-fold in low Fe (SL) and 2.45-fold in low light (+Fe) compared to the control (Fig. 5; for detailed $\log_2$FC and CPM values in each treatment, *see* Supporting Information Table S4). The expression of the PSI KEGG module was likely driven by the expression of *PsaE*, a gene encoding a PS1 subunit, which was overrepresented 7.7-fold under low Fe (SL) and 4.1-fold under low light (+Fe) (Fig. 4; for detailed $\log_2$FC and CPM values in each treatment, *see* Supporting Information Table S5). PsaE does not require Fe, but may be helpful in maintaining the structural integrity of the PSI complex, or in avoiding electron leakage to oxygen, thereby preventing the formation of reactive oxygen species (ROS) (Jeanjean et al. 2008). Similar expression patterns were detected with genes encoding subunits of PSII (*PsbO*, *PsbP*) in which they were overrepresented in the low iron and/or low light treatment despite the larger complex overall being underrepresented relative to the control (Fig. 4). These expression patterns indicate that while both photosystem complexes are working collaboratively under stressful conditions to create a proton gradient for ATP synthase, albeit at a slower rate, individual subunits likely have unique, important functions under low iron and/or low light to maintain the efficiency of photosynthesis.

Substantial expression changes were seen in the iron-rich components of photosynthesis as well as their iron-free equivalents. The gene encoding for cytochrome b_6f iron-sulfur subunit (*PetC*) was underrepresented in low Fe (SL, LL) (Fig. 4), but not significantly overrepresented under low light (+Fe), although it was most abundant in this treatment (Fig. 3B—top of triangle). PetC functions to transfer electrons between the two reaction center complexes but can be replaced with the copper-containing plastocyanin (PCYN) when the cell is iron-limited (Peers and Price 2006). *F. kerguelensis* contains three isoforms of *PCYN*, more than all other diatoms sequenced in the MMETSP transcriptomes (Groussman et al. 2015). We observed two different expression responses; *PCYN-2b* was overrepresented 8.8-fold under low Fe (SL) and > 18-fold under low light (+Fe, −Fe), indicating a general stress response with particular sensitivity to light level (Fig. 4). Two other isoforms, *PCYN-2a* and *-3*, appeared sensitive to iron status, but transcripts were only weakly overrepresented in low Fe (SL, LL) (Fig. 4) and were not as abundant as *PCYN-2b* (Fig. 3B—bottom portion of triangle). Both of these isoforms were underrepresented in low light (+Fe), suggesting substantial dependence on *PCYN-2b* in low light scenarios.

Transcripts for ferredoxin (*PetF*), an iron-containing photosynthetic electron transfer protein, were not detected in any

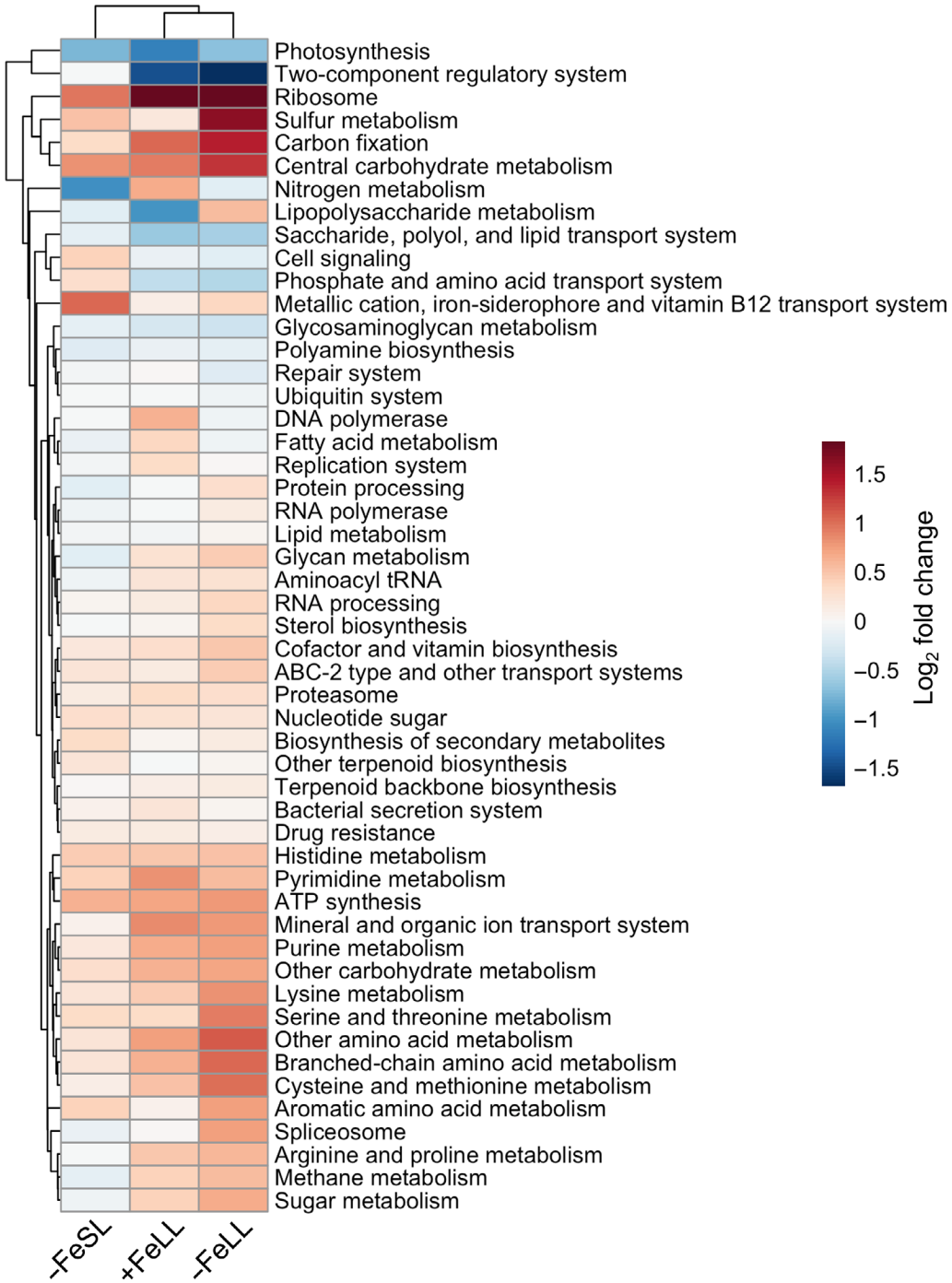

Fig. 2. Differential expression response of broad KEGG Class 3 categories in *F. kerguelensis*. Heatmap represents the $\log_2$ fold-change of KEGG Class 3 categories within each treatment (−FeSL, +FeLL, −FeLL) relative to the control (+FeSL). Warmer colors indicate overrepresented categories and cooler colors indicate underrepresented category annotations. Dendrogram clustering of treatments and categories are based on Euclidean distances.

of our transcriptomes; however, we detected transcripts for two isoforms of flavodoxin (*FLDA*), an iron-free equivalent to PetF; one isoform of *FLDA1*, and two paralogs of the *FLDA2* isoform (Fig. 4). Transcripts for *FLDA2a* and *FLDA1* were overrepresented > 2.8-fold ($p < 0.03$) in low Fe (SL), > 4.2-fold in low light (+Fe), and > 9.4-fold in low Fe/low light (−FeLL), suggesting an additive effect of iron and light limitation on *FLDA* isoform gene expression (Fig. 4). The most differentially expressed gene in our study was *FLDA2b*, which was highly overrepresented in low Fe (SL, LL) ($\log_2$ FC = 10.9), as transcripts were barely detected in iron-replete cells (Fig. 3B—bottom axis of triangle). The replacement of PetF with FLDA

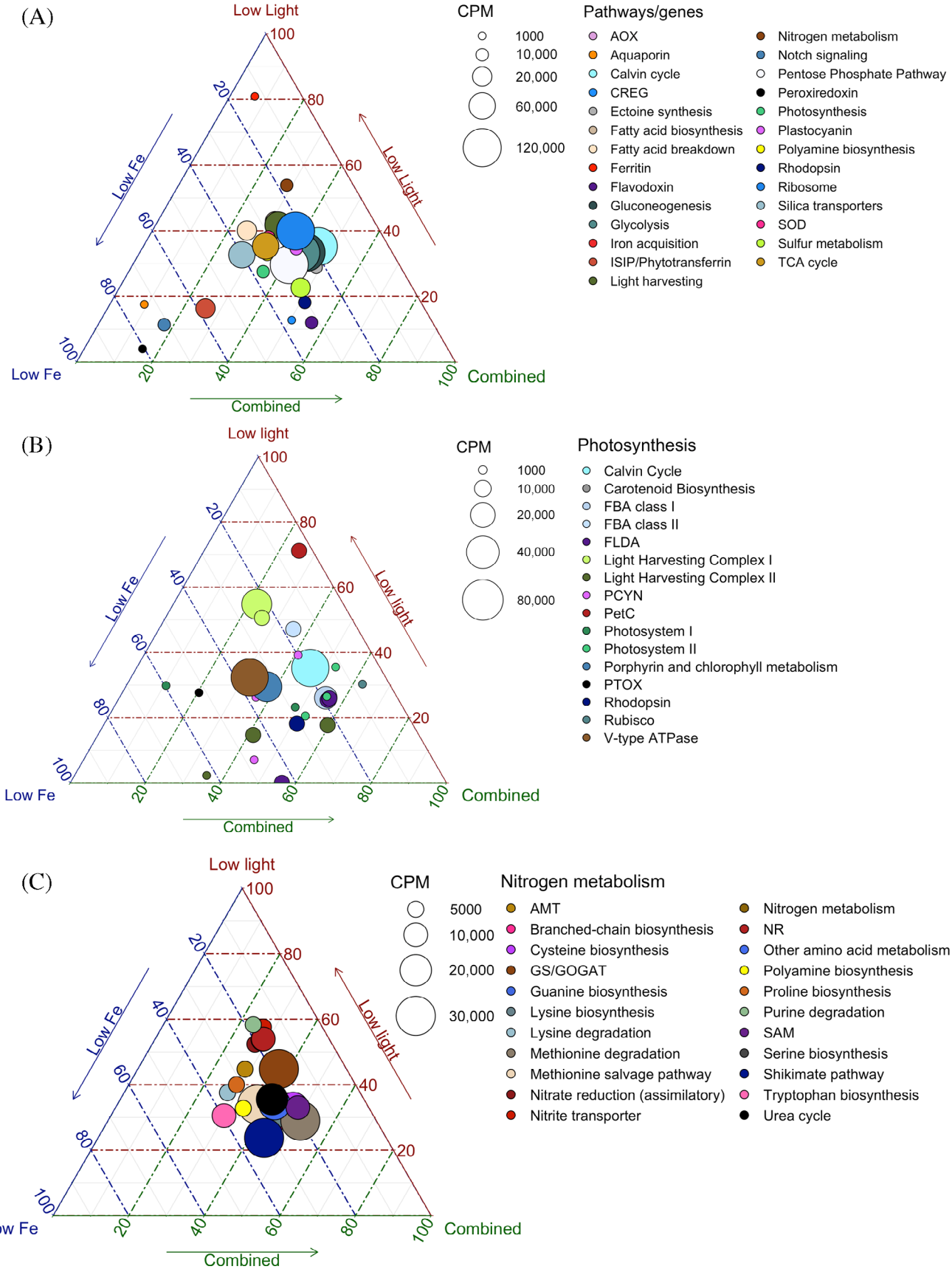

Fig. 3. Legend on next page.

has been documented in many laboratory and field studies and has been proposed as a molecular indicator of iron limitation (La Roche et al. 1996; Allen et al. 2008; Chappell et al. 2014). As observed here, *F. kerguelensis* may rely heavily on *FLDA2b* when iron-limited and *FLDA2a* and *FLDA1* when light limited. Although not detected in our transcriptomes, *F. kerguelensis* could possess a *PetF* gene, as in the case of the recently sequenced genome of the sea-ice diatom *Fragilariopsis cylindrus* (Mock et al. 2017); however, *F. kerguelensis* may be permanently adapted to using diversified copies of *FLDA* that are responsive to different types of stressors as an important strategy to survive under rapidly changing iron and light regimes. Indeed, a dependence on iron-free electron transfer proteins such as PCYN and FLDA appears to be more common in SO diatoms than in non-SO diatoms (Moreno et al. 2018).

Proteorhodopsins (PRs) may serve as another low iron and light mitigation strategy that *F. kerguelensis* utilizes under stress. PRs are common in diatoms residing in SO waters and other HNLC regions (Marchetti et al. 2015), but unlike iron-rich photosynthesis complexes, PRs can absorb light energy to create a proton gradient across cell membranes for ATP synthesis without an associated high iron requirement (Kloer et al. 2005; Marchetti et al. 2015). Additionally, the photoisomerization reaction within PRs, transporting H^+ ions across membranes, is likely insensitive to low temperatures, whereas photosynthesis and respiration rates decrease with temperature (Strzepek et al. 2019). Therefore, SO diatoms may use PRs to supplement the energy demands of the cell. Transcripts for a gene encoding a rhodopsin (*RHO*) were overrepresented 15.8-fold in low light (+Fe), 25.5-fold in low Fe (SL), and 46.5-fold in low Fe/low light (−FeLL) (Fig. 4). RHO appears to be part of a general stress response in *F. kerguelensis*, with an additive interaction between iron and light limitation on *RHO* gene expression; the highest CPMs were also detected in the −FeLL treatment (Fig. 3B). *F. cylindrus RHO* was similarly overrepresented to varying degrees under several types of growth-limiting conditions (Strauss 2012), and RHO gene and protein expression in the oceanic diatom *Pseudo-nitzschia granii* was shown to be most sensitive to iron status (Marchetti et al. 2015). RHO is likely an integral part of maintaining the energy demands of *F. kerguelensis* and perhaps other SO diatoms.

Reorganization of the light harvesting machinery is an important acclimation strategy to cope with variable iron and light conditions. Similar to expression patterns within photosynthesis, transcript abundances of light-harvesting complex Chl *a/b*-binding protein (LHC) varied in relation to both iron and light availability. The LHC complex I genes, particularly LHC complex I protein 1, were influenced by light availability, being the most abundant and overrepresented under low light (+Fe) (Fig. 3B). Light-harvesting transcripts were overrepresented in sea-ice phytoplankton relative to pelagic communities along the Western Antarctic Peninsula (WAP) (Pearson et al. 2015). An LHC complex stress-related I gene in *Phaeodactylum tricornutum* was shown to be highly expressed in low-light acclimated cells, providing the diatom with a high nonphotochemical quenching capacity, which could be useful under fluctuating or high light conditions (Bailleul et al. 2010). On the other hand, transcripts for LHC complex II genes were overrepresented under low Fe (SL, LL) (Fig. 3B), in parallel with findings from previous transcriptome studies of iron-limited diatoms (Allen et al. 2008; Lommer et al. 2012). In particular, LHC complex II binding protein 6 demonstrated sensitivity to iron status as it was overrepresented > 7.1-fold under low Fe (SL, LL), and only a few transcripts were detected in low light (+Fe) (Fig. 4).

SO phytoplankton have been shown to have large amounts of Chl *a* per photosystem and comparably larger absorption cross-sections, even under iron limitation (Strzepek et al. 2012). Many phytoplankton maintain a large percentage of their chlorophyll and light harvesting complexes despite experiencing severe iron deprivation (Moseley et al. 2002; Allen et al. 2008). *F. kerguelensis* did not highly regulate chlorophyll and porphyrin metabolism, but did appear to utilize chlorophyll and iron recovery and maintenance strategies. Transcripts that may be involved in plastid iron homeostasis include a heme oxygenase (*HO*), a ferrochelatase (*HEMH*), and a putative bilin oxidoreductase-encoding enzyme (*PebA*). While only weakly overrepresented, these transcripts suggest a role in the synthesis (HEMH) and breakdown (HO) of heme in order to recover iron from damaged porphyrins (Marchetti and Maldonado 2016). The breakdown of heme to free iron also yields bilirubin IX-alpha (BV), and the increased expression of *PebA* may suggest that BV acts as the chromophore for

Fig. 3 Ternary plot derived from normalized CPM gene expression data from the three treatments for (**A**) overall metabolisms and selected genes, (**B**) photosynthesis, and (**C**) broad nitrogen metabolisms. The size of each circle indicates the CPM of a gene or module, whereas the position of the circles represents the relative abundance of the gene or module in each treatment. Blue lines within ternary plot denote 20% increments of the total contribution of reads from the low Fe treatment. The direction of the blue arrow indicates the increase in relative contribution toward 100%. Similarly depicted for the low light treatment (red axis) and the low Fe/low light treatment (green axis). Transcripts that are equally abundant in all three treatments will be located toward the center of the triangle, whereas those found near the corners indicate higher relative abundance in that treatment than in the other two treatments. Circles located on triangle sides denote genes or modules with higher relative abundance in the two treatments at those corners that are not present in the treatment of the opposite corner. AOX, mitochondrial alternative oxidase; CREG, cellular repressor of E1-A gene; SOD, superoxide dismutase; FBA, fructose bisphosphate aldolase; FLDA, flavodoxin; PCYN, plastocyanin; PetC, cytochrome b_6f complex Fe-S subunit; PTOX, plastid terminal oxidase; AMT, ammonium transporter; GS/GOGAT, glutamine synthase/ferredoxin glutamate synthetase; NR, nitrate reductase NAD(P)H; SAM, s-adenosylmethionine synthetase.

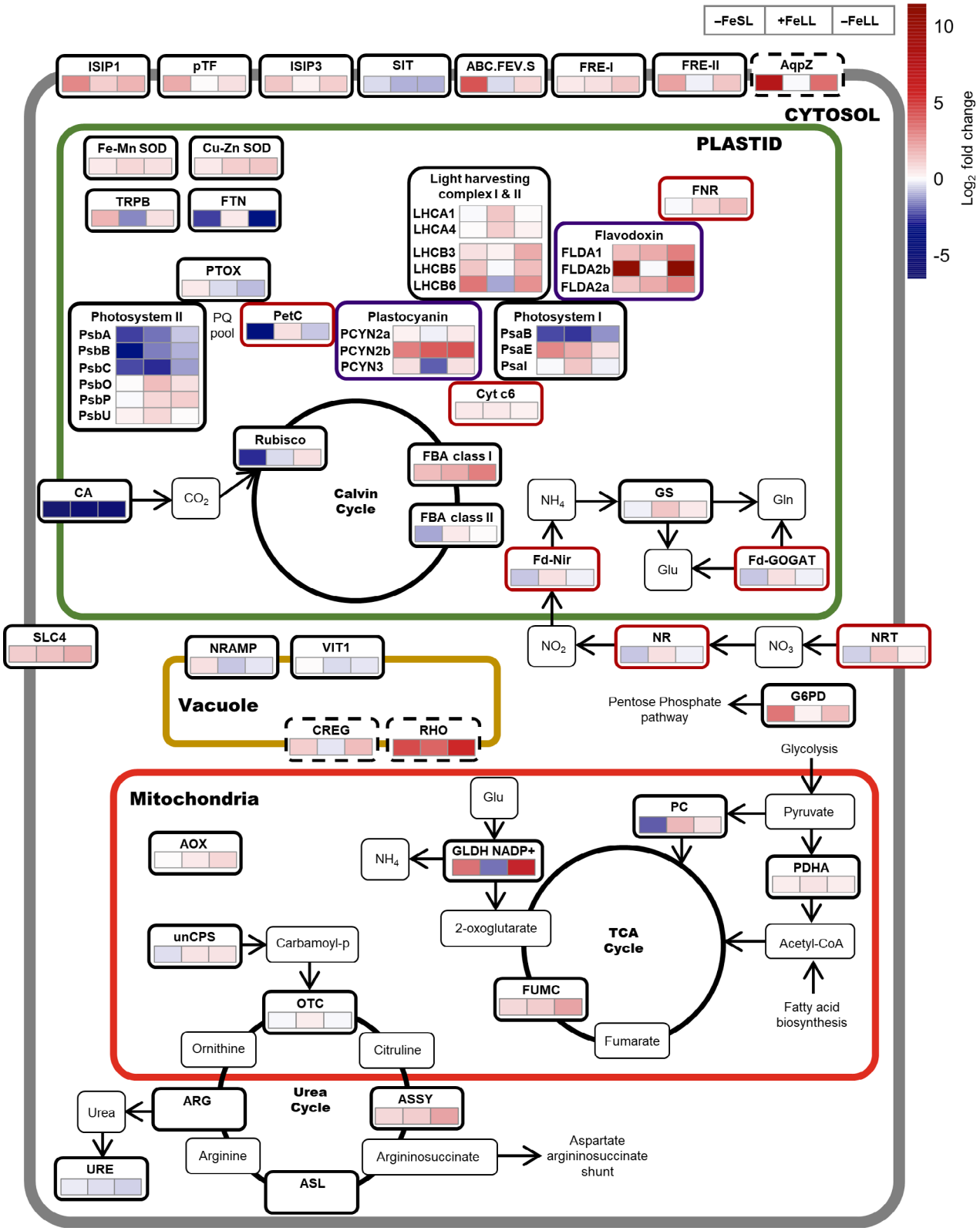

Fig. 4. Legend on next page.

diatom phytochrome, which senses red/far-red light in the ocean (Fortunato et al. 2016). Even while severely energy limited, *F. kerguelensis* appears to allocate resources to chlorophyll and pigment maintenance and/or degradation that may enable the cell to cope under low iron and/or low light conditions.

Iron acquisition and homeostasis

Diverse iron metabolism proteins are critical in helping the cell maintain growth during periods of iron limitation. One strategy that may be particularly helpful is luxury uptake of iron beyond what is needed for the cell to achieve maximum growth rates (Marchetti et al. 2009). Iron storage proteins such as ferritins (FTN) safely store iron to minimize potential cell damage from ROS and oxidative stress via iron-mediated Fenton chemistry (Imlay 2008). *F. kerguelensis* uses FTN to generate iron reserves for subsequent cell growth when iron levels decline to growth-limiting concentrations and has been proposed as a molecular indicator of iron status in polar diatoms (Marchetti et al. 2017). *F. kerguelensis FTN* was significantly underrepresented by fivefold and ninefold in low Fe (SL) and in low Fe/low light (−FeLL), respectively (Fig. 4). Transcripts for FTN were most abundant in the +Fe (LL) treatment (Fig. 3A). Considering ephemeral iron inputs into the SO, storing iron when it is available is likely a critical strategy to their survival.

Numerous strategies for acquisition of organically complexed iron have been documented in model diatoms, but those specifically invoked by *F. kerguelensis* are unknown. At the KEGG Class 3 level, *F. kerguelensis* overrepresented the metallic cation iron-siderophore and vitamin B_{12} transport system under low Fe (SL) compared to the control (Fig. 2). At the module level, this diatom overrepresented the "iron complex transport system" and the "iron-starvation induced protein (ISIP)" modules, indicating the cell was activating iron-acquisition and trafficking machinery (Fig. 5A,C). Many laboratory and field based studies have documented overrepresentation of a phytotransferrin (pTF) protein (McQuaid et al. 2018), previously iron starvation-induced protein 2a (*ISIP2a*), under iron limitation (Lommer et al. 2012; Marchetti et al. 2012; Cohen et al. 2017*b*). This gene is a high-affinity Fe(III) concentrating protein (Morrissey et al. 2015; McQuaid et al. 2018) and is likely an important mechanism by which *F. kerguelensis* acquires iron as it was overrepresented 4.2-fold and highly abundant in low Fe (SL); however, the increase in low Fe/low light (−FeLL) was not significant (Fig. 4).

The function of iron starvation-induced protein 1 (*ISIP1*) in the uptake of iron-siderophore complexes has recently been demonstrated (Kazamia et al. 2018), but the function of ISIP3, another iron response gene, remains mostly unknown (Lommer et al. 2012; Marchetti et al. 2012; Morrissey et al. 2015; Cohen et al. 2017*b*). *ISIP3* shared similar expression patterns to *pTF* in that it was overrepresented 2.6-fold in low Fe (SL) ($p = 0.03$), whereas the increase in low Fe/low light (−FeLL) was not significant. *ISIP1* was overrepresented in all treatments, but appeared most sensitive to iron status, being overrepresented sevenfold in low Fe (SL) and 3.6-fold in low Fe/low light (-FeLL) (Fig. 4). While the distribution of *pTF* and *ISIP3* genes appears cosmopolitan throughout the world's oceans, *ISIP1* is more common in SO diatoms (Moreno et al. 2018) and may enable *F. kerguelensis* to take up and use hydroxamate siderophores via endocytosis (Kazamia et al. 2018). Gene expression patterns of *pTF* and *ISIP3* have been proposed as molecular indicators of iron limitation in diatoms, but expression of *ISIP1* could also serve as an indicator for iron status in *F. kerguelensis*, and perhaps other polar diatoms, as it appears to be specific to iron limitation regardless of light level.

In further support that nonreductive iron acquisition via ISIPs is a primary strategy employed by SO diatoms, many SO diatoms do not appear to contain a complete high-affinity Fe(III) uptake system (Groussman et al. 2015; Moreno et al. 2018). The *F. kerguelensis* transcriptome does not include transcripts for an iron permease, but does contain two copies of iron reductase (*FRE*), more than most other MMETSP diatoms. One copy (*FRE1*) was overrepresented greater than twofold ($p = 0.04$) in low Fe/low light (−FeLL), and the second copy (*FRE2*) was > 2.62 overrepresented in low Fe (SL, LL) ($p < 0.04$); however, the

Fig. 4 Simplified cell schematic visualizing select genes of interest and their expression changes in N, C, Fe, and metal transport/assimilation processes within *F. kerguelensis*. Colored squares indicate $\log_2$ fold-change in each treatment vs. the control with red representing higher expression under treatment conditions and blue representing higher expression under Fe-replete control conditions. Red outlines of genes indicate an Fe-requiring protein. Purple outlines indicate Fe-free equivalents. Dashed outlines indicate putative cellular localization. Empty boxes indicate genes that had low sequence abundance or were not detected in the transcriptome. [Plastid] PsbA, photosystem II P680 reaction center D1 protein; PsbB, photosystem II CP47 chlorophyll apoprotein; PsbC, photosystem II CP43 chlorophyll apoprotein; PsbO, photosystem II oxygen-evolving enhancer protein 1; PsbP, photosystem II oxygen-evolving enhancer protein 2; PsbU, photosystem II PsbU protein; PsaB, photosystem 1 P700 Chl *a* apoprotein A2; PsaE, photosystem 1 subunit IV; PsaI, photosystem I subunit VIII; PTOX, plastid terminal oxidase; PetC, cytochrome b_6f complex Fe-S subunit; FNR, ferredoxin-NADPH reductase; CA, carbonic anhydrase; FBA, fructose bisphosphate aldolase; Fd-Nir, ferredoxin-nitrite reductase; GS, glutamine synthetase; Fd-GOGAT, ferredoxin glutamate synthetase; FTN, ferritin; Fe-Mn SOD, Fe/Mn superoxide dismutase; Cu-Zn SOD, Cu/Zn superoxide dismutase; TRPB, tryptophan synthase beta chain; [Mitochondria] AOX, mitochondrial alternative oxidase; ARG, arginase; ASSY, arginosuccinate synthase; ASL, arginosuccinate lyase; FUMC, fumarate hydratase; GLDH-NADP+, NADP+ dependent glutamate dehydrogenase; OTC, ornithine carbamoyltransferase; PC, pyruvate carboxylase; PDHA, pyruvate dehydrogenase E1 component; unCPS, carbamoyl-phosphate synthase. [Cytosol] NRT, MFS transporter, NNP family, nitrate/nitrite transporter; NR, nitrate reductase NAD(P)H; G6PD, glucose-6-phosphate dehydrogenase; SLC4, solute carrier protein; [Vacuole] CREG, cellular repressor of E1-A gene; NRAMP, natural resistance-associated macrophage protein; RHO, rhodopsin; VIT1, vacuolar iron transporter.

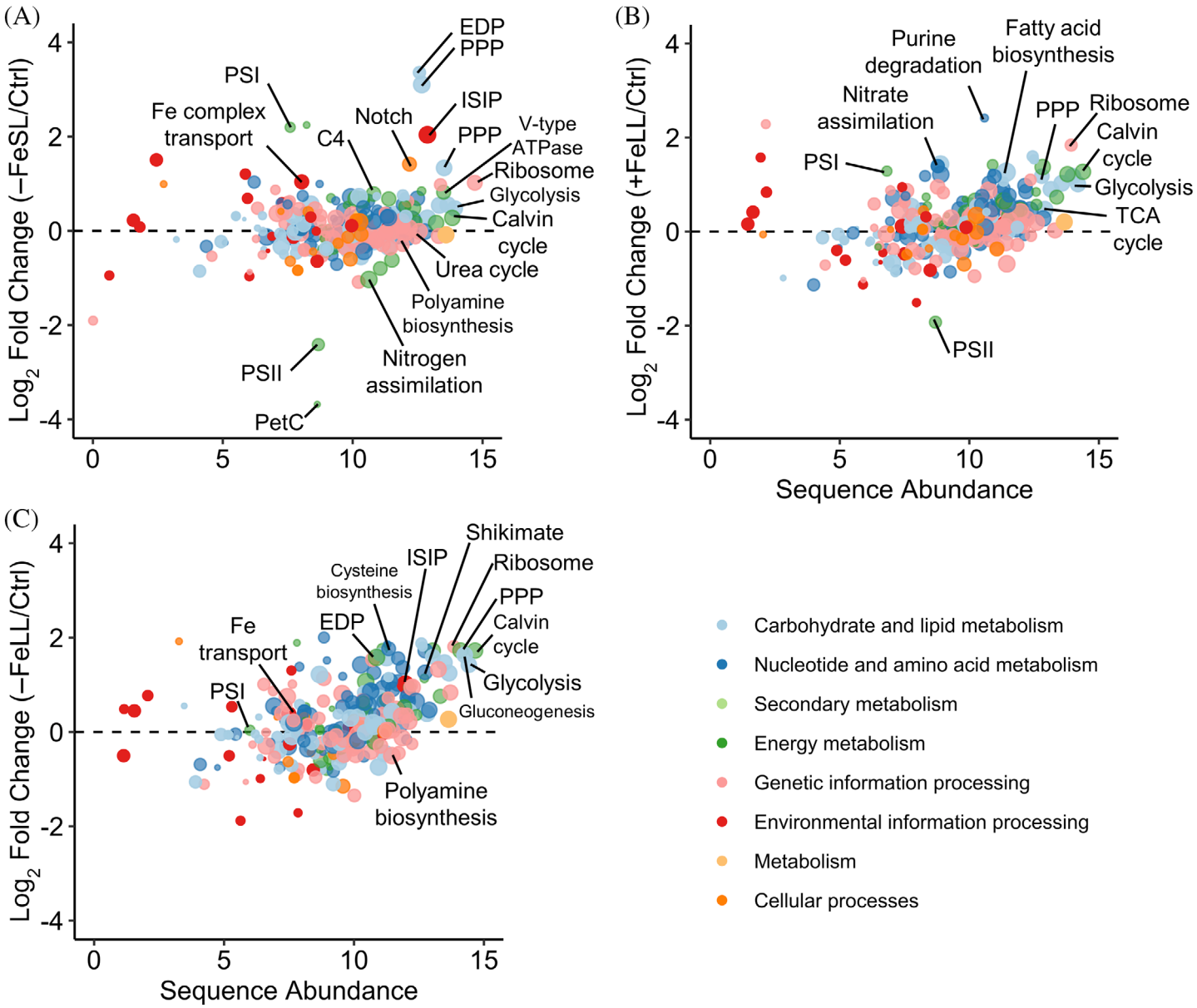

Fig. 5. Metabolic pathway expression differences between each of the low Fe and/or low light treatments relative to the control in *F. kerguelensis*. Scatter plots are $\log_2$ fold-change of module transcripts for the treatment relative to the control (+FeSL) vs. average sequence abundance (logCPM) in (**A**) the low Fe treatment (−FeSL), (**B**) the low light treatment (+FeLL), and (**C**) the combined low Fe/low light treatment (−FeLL). Colors represent modules that are grouped into eight broader categories of different metabolic functions. Circle size indicates the percentage of enzymes/proteins with transcripts that hit on that KEGG module. Selected modules are annotated, including: PSI, photosystem I; PSII, photosystem II; EDP, Entner-Doudoroff pathway; ISIP, iron starvation induced proteins (includes *ISIP1*, *ISIP3*, and *pTF*); PPP, pentose phosphate pathway; PetC, cytochrome b_6f complex Fe-S subunit; TCA, tricarboxylic acid cycle.

transcript abundance of *FRE2* was low (Fig. 4). In addition to Fe(III) transporters, transcripts for divalent metal transporters belonging to the *ZIP* and *NRAMP* families were detected in *F. kerguelensis*. NRAMP is thought to transport metals out of vacuolar storage and has been hypothesized to function similarly in centric diatoms (Kustka et al. 2007; Nuester et al. 2012), but in *F. kerguelensis* it was only weakly overrepresented in the low Fe (SL) treatment. A ZIP transporter was overrepresented under all conditions compared to the control, but had low transcript abundances. We hypothesize that the high-affinity iron uptake system, NRAMP, and ZIP may not be primary strategies that *F. kerguelensis* employs, but may still be useful under certain environmental conditions.

Finally, an ATP binding cassette (ABC)-type ferric iron transporter (*ABC.FEV.S*) was identified in *F. kerguelensis* and was significantly overrepresented in all treatments compared to the

control, but appeared to be more sensitive to iron limitation being overrepresented sixfold and fourfold in low Fe (SL) and low Fe/low light (−FeLL), respectively (Fig. 4). *ABC.FEV.S* was similarly expressed in diatom metatranscriptomes from a low iron WAP region (Pearson et al. 2015) and in iron-limited *Thalassiosira* from the California upwelling system (Cohen et al. 2017*b*), suggesting its usefulness under low iron scenarios. As iron-limited *F. kerguelensis* decrease growth rates and Chl *a* contents, cells maintain low iron quotas (Fe:C), low half saturation values (K_m) for growth with respect to iron, and have high iron use efficiencies (Timmermans et al. 2004; Hoffmann et al. 2007; Marchetti and Cassar 2009; Strzepek et al. 2011), likely through a reliance on distinct molecular strategies. Given their sensitivity to iron status in laboratory cultures and in the field, we hypothesize *FTN*, *pTF*, *ISIP1*, and *ABC.FEV.S* may play critical roles in maintaining growth during periods of low iron conditions and could be used as molecular indicators for iron limitation in the field. Additional characterization is needed to clarify their specific roles in binding, transporting and delivering iron to iron-demanding intracellular processes.

Mechanisms to reduce ROS under low iron/low light conditions

Metabolic imbalances between photosynthesis, photorespiration, and alternative oxidative pathways can be exacerbated by nutrient limitation, extremely low temperatures, increased solubility of oxygen in polar oceans, and UV damage. Therefore, *F. kerguelensis* must use a broad spectrum of antioxidant enzymes to protect its cellular machinery against ROS. Due to iron limitation, ROS defense proteins that require iron as a catalytic cofactor can be inhibited, thereby increasing dangerous ROS levels in the cell (Allen et al. 2008). The increased abundance of transcripts associated with serine, glycine, and threonine metabolism (Fig. 2), mainly under the low Fe/low light (−FeLL) condition, suggests intensified photorespiration and increased ROS levels (Davis et al. 2016). If so, *F. kerguelensis* must have effective mechanisms for removing excess electrons for scavenging ROS that are produced as a consequence of these processes (Peers and Price 2004).

Iron limitation can generate ROS in the mitochondria from an iron-compromised electron transport chain, yet *F. kerguelensis* did not highly express alternative mitochondrial oxidase (AOX), Fe-Mn superoxide (*SOD*), or Cu-Zn *SOD* (Fig. 4) as do other diatoms, such as *P. tricornutum* and *Thalassiosira pseudonana* (Peers and Price 2004; Allen et al. 2008; Bailleul et al. 2015). Because regulating the traffic of reducing equivalents between mitochondria and plastids is important, *F. kerguelensis* likely possesses an additional set of ROS mitigation strategies in these organelles. Iron and heme-free antioxidant enzyme-encoding genes increased in expression under low iron conditions, presumably to replace other ROS scavenging functions. A chloroplast, non-heme-containing peroxiredoxin (PrxQ) using thioredoxin as an electron donor to detoxify various peroxide substrates (Laxa et al. 2007) was overrepresented 13.5-fold under low Fe (SL) and twofold (p = 0.02) in low Fe/low light (−FeLL), but was barely detected under low light (+Fe) (Fig. 3A). In *Arabidopsis thaliana*, PrxQ is targeted to plastids and functions to protect PSII (Lamkemeyer et al. 2006). In *F. kerguelensis*, PrxQ may serve a similar antioxidant function for PSII under low iron conditions. The expression of *PrxQ* may also depend on the extent of iron limitation, whether being a short- or long-term acclimation. Studies on the effects of temperature stress on corals have shown that heat shock proteins are expressed in the early stages of acclimation while peroxiredoxins are expressed during longer acclimation periods (Portune et al. 2010; Meyer et al. 2011). It may be possible that *F. kerguelensis* relies on *PrxQ* under extreme low iron/low light scenarios to avoid photoinhibition.

Under all stressed conditions, but particularly iron limitation, a *myo*-inositol dehydrogenase (InDH) was overrepresented 14.2-fold under low Fe (SL), and 16.1-fold under low Fe/low light (−FeLL). Similar expression patterns of this gene under iron limitation were observed in *P. tricornutum* (Allen et al. 2008) and *F. cylindrus* (Strauss 2012). *Myo*-inositol is incorporated into cellular structures by interacting with membranes, proteins, and enzymes (Valluru and Van den Ende 2011) and was also found to be in higher cellular concentrations in *P. tricornutum* under iron stress (Allen et al. 2008). As red algal mitochondria can use *myo*-inositol for respiration, it was proposed that InDH is involved in a mitochondrial inositol/inosase shuttle system for reducing equivalents in chromalveolates and red algae (Gross and Meyer 2003). InDH has also been proposed to be involved in mitigating ROS production along with the use of AOX and NADH dehydrogenase systems (Allen et al. 2008; Kroth et al. 2008). This may be a strategy that *F. kerguelensis* relies on more than *AOX* or an NADPH dehydrogenase system, as these enzymes were not significantly overexpressed. Nevertheless, InDH has broad associations with signal transduction, hormone regulation, and stress tolerance and could be involved in other aspects of carbohydrate metabolism (Kroth et al. 2008).

Amino acid and protein metabolisms

Iron and light limitation invoked a dramatic response from ribosome, amino acid (cysteine, methionine, and branched-chain), and sulfur-based metabolisms in the transcriptome of *F. kerguelensis*. Several amino acid pathways and genes were overrepresented under low light (+Fe, −Fe), including branched-chain amino acids (BCAAs), cysteine and methionine metabolism, and other amino acid metabolisms at the KEGG Class 3 category level (Fig. 2). Located in the plastid, BCAAs are synthesized de novo from pyruvate, 2-oxobutanoate and acetyl-CoA, and are associated with protein repair and signaling (Smith et al. 2016). Several intermediate steps in the BCAA biosynthesis pathway were overrepresented, especially under low Fe/low light (−FeLL), including a ketol-acid reductoisomerase (ilvC) and 3-isopropylmalate dehydrogenase (leuB) (p = 0.03),

which were overrepresented by fivefold and twofold, respectively. These transcripts indicate that synthesis of valine and isoleucine may be important when the chloroplast is energy-limited, but these enzymes also catalyze reverse reactions. More likely, BCAA catabolism may be important under stressful conditions as it could provide energy-limited cells labile sources of carbon and chemical energy via pyruvate.

A diversity of enzymes involved in amino acid pathways could contribute to recycling of intracellular carbon and nitrogen, forming new amino acids or even ammonium or pyruvate. Aromatic amino acids (AAAs) are formed via the shikimate pathway and include phenylalanine, tryptophan, and tyrosine, which are important precursors to numerous pigments, hormones, and cell wall components (Bromke 2013). The shikimate pathway was weakly overrepresented under low Fe/low light (−FeLL) conditions (Fig. 5C), while tryptophan biosynthesis was not overrepresented in any treatment. However, transcripts for the enzyme that catalyzes the last step of the pathway, tryptophan beta synthase (TrypB), were overrepresented threefold under low Fe (SL) (Fig. 4). Tryptophan biosynthesis is energetically costly, but TrypB may confer quenching of variable fluorescence of chlorophyll at the D2 protein of PSII under high light as was observed in a cyanobacteria (Vavilin et al. 1999; Allen et al. 2008), perhaps explaining the higher expression of this gene under low Fe (SL). The increased expression of the shikimate pathway could also be explained by the synthesis of mycosporine-like amino acids (MAAs), which play a role in protecting against UV radiation as well as having other possible functions as antioxidants and osmolytes (Llewellyn and Airs 2010); however, biosynthetic enzymes that produce MAAs, and the genes that encode them are putative and were not identified in the *F. kerguelensis* transcriptome.

Major shifts in the transcription of genes involved with sulfur-containing cysteine and methionine biosynthesis pathways were also induced under the low Fe/low light (−FeLL) condition (Fig. 2). Iron and sulfur are required in stoichiometric proportions to synthesize Fe-S clusters, indicating the two pathways must be tightly regulated in order to meet the changing nutrient status of the cell while also potentially avoiding free iron and sulfur in organelles, which could be toxic (Giordano et al. 2005). After the reduction of sulfate, almost all sulfur in the cell is incorporated into cysteine, serving as a precursor for the biosynthesis of methionine, Fe-S clusters, and the redox compound glutathione (Giordano et al. 2005). Methionine is used to synthesize S-adenosyl-L-methionine (SAM), an important methylating agent, propylamine donor, and radical source (Bertrand et al. 2012). In all treatments, but particularly evident under low iron/low light (−FeLL), we observed an overrepresentation of sulfur metabolism genes at the KEGG Class 3 level (Fig. 2), as well as those involved in methionine degradation and cysteine biosynthesis (Figs. 3C, 5C). Apparently, *F. kerguelensis* increases the capacity to synthesize and/or catabolize cysteines and methionines under low iron and/or low light conditions compared to iron-replete conditions. Upregulation of these pathways could be a response to elevated oxidative stress as ROS are more likely to target proteins that contain sulfur-containing amino acids and thiol groups, such as Fe-S clusters and cysteines (Berlett and Stadtman 1997). Alternatively, an upregulation of cysteine and methionine catabolism does not rely on NADH and could provide N in the form of recycled ammonium deaminated by a methionine-gamma-lyase (Hildebrandt et al. 2015). Highlighting this dual shift in amino acid synthesis and degradation, we observed transcripts of methionine-gamma-lyase (*MGL*) and SAM synthetase (*METK*) to be overrepresented 3.6-fold and 3.7-fold in low Fe/low light (−FeLL), respectively. The increased expression of *METK* suggests that DNA methylation may be a strategy that provides diatoms the plasticity they need to coordinate responses to abiotic stress, such as, low iron, cold temperatures, or variable salinity. In *P. tricornutum*, DNA methylation affected the expression of over 300 genes (Veluchamy et al. 2013) and in *T. pseudonana*, transcription factors were found to control regulatory networks of thousands of coexpressed genes in response to a shift from nutrient replete to limiting conditions (Ashworth et al. 2013). Methionine synthase is also a precursor to dimethylsulfoniopropionate (DMSP), but expressed genes for the pathway were absent in the *F. kerguelensis* transcriptome.

Nitrogen recycling and alternative carbon metabolisms

Nitrogen assimilation is an iron-dependent and energetically demanding process, driven by reducing power derived from photosynthesis or from the catabolism of protein and carbon reserves. Genes encoding proteins that require iron and reducing equivalents to assimilate nitrate were weakly overrepresented under low light (+Fe), including a cytosolic nitrate reductase (*NR*), a nitrite reductase (*NirA*), and a nitrate transporter (*NRT*) (Fig. 4). Although N assimilation was mostly underrepresented under low iron conditions (Figs. 3C, 5B), it may be possible for the cell to maintain N demands by scavenging N from amino acids (Rokitta et al. 2014).

Ammonium and glutamate are converted into glutamine by the activity of glutamine synthetase (*GS*) and ferredoxin-glutamate synthase (*Fd-GOGAT*), a key step in the biosynthesis of amino acids and other nitrogenous compounds (Hockin et al. 2012). Both GS ($p = 0.03$) and Fd-GOGAT ($p = 0.03$) were overrepresented ~ 2.5-fold under low light (+Fe) (Fig. 4). The mitochondrial matrix enzyme NADP+ dependent glutamate dehydrogenase (*GLDH NADP+*) was overrepresented 32-fold under low Fe/low light (−FeLL) (Fig. 4), and catalyzes the oxidative deamination of glutamate to free ammonium and 2-oxoglutarate for subsequent use in the tricarboxylic acid (TCA) cycle. A GLDH shunt would enable the release of carbon skeletons from amino acids and serve as an intersection between carbon and nitrogen metabolisms (Hildebrandt et al. 2015). In support of this shunt, it appears the amino groups of methionine and cysteine are released as ammonium during the deamination reactions performed by methionine gamma

lyase, as previously mentioned. These changes in N metabolism under iron limitation are similar to those observed in other diatoms and phytoplankton experiencing N limitation (Allen et al. 2011; Hockin et al. 2012; Rokitta et al. 2014), and it may be that the expression of N assimilation transcripts is more affected by growth rate than by iron or light status.

The ornithine-urea cycle (OUC) is an important hub of nitrogen and carbon redistribution in diatoms (Allen et al. 2011); however, in *F. kerguelensis*, the expression of protein-encoding genes involved in OUC appear to be weakly regulated with most of the genes either not significantly differentially expressed or in very low abundances. The genes encoding argininosuccinate synthase (*ASUS*) and arginase (*ARG*) were weakly overrepresented in all treatments compared to the control, significantly increasing in low Fe/low light (−FeLL) by 3.5-fold and threefold, respectively. Transcripts for the latter half of the cycle were not detected (Fig. 4). This may suggest that argininosuccinate produced in the first half of OUC is returned to the TCA cycle as malate in the aspartate-argininosuccinate shunt proposed by Allen et al. (2011). More differentially expressed genes detected at the beginning of the cycle rather than in subsequent steps has also been observed in *T. pseudonana* (Hockin et al. 2012), *P. tricornutum* (Allen et al. 2011), and in the coccolithophore *Emiliania huxleyi* (Rokitta et al. 2014). Differential regulation within a metabolic pathway may be the result of post-transcriptional and post-translational regulation, or it may be attributed to allosteric regulation of enzymes in response to changes in nutrient availability (Hockin et al. 2012). Pathways that connect the urea cycle with proline and polyamine synthesis, as well as genes such as spermine/spermidine synthase, were not strongly regulated (Fig. 3C). Because decreased enzyme activity may lead to increased metabolite pool sizes, it might be they still have important roles as osmolytes and cell wall components. While some N intermediates may be important to the TCA cycle, it appears that in *F. kerguelensis* amino acid pathways may serve as a better N recycling strategy during iron and/or light limitation than nitrate assimilation or the urea cycle.

Carbon metabolism genes were investigated to determine the role of carbon fixation, glycolysis, the pentose phosphate pathway (PPP), and the TCA cycle. Diatoms have multiple carbon concentrating mechanisms (CCMs) used to concentrate CO_2 near the RuBisCO enzyme within the plastid. One method is based on the action of carbonic anhydrases (*CA*) and the other is based on the delivery of CO_2 to the plastid by the decarboxylation of C4 compounds (Kroth et al. 2008). *CA* was underrepresented by > 50-fold in all treatments compared to the control; however, a solute carrier (*SLC4*) associated with the CCM of the plasmalemma that transports bicarbonate (Nakajima et al. 2013), was weakly overrepresented in all treatments (Fig. 4). It is also possible that aquaporins (*AQP*), that is, water/ion channels that putatively transport Si or CO_2/NO_3^-, are able to transport CO_2 to the plastid in addition to *SLC4* (Matsuda et al. 2017). AQP-Z was 188-fold overrepresented in the low Fe (SL) treatment and was one of the most highly expressed genes in this study (Fig. 4). Diatoms may have the ability to carry out C4 metabolism which would be helpful with excess energy dissipation and/or cellular pH homeostasis; however, research has demonstrated inefficient inorganic carbon cycling and ATP production via C4 (Kroth et al. 2008; Reinfelder 2011; Haimovich-Dayan et al. 2013). C4 metabolism pathway genes were slightly overrepresented in all three treatments relative to the control (Supporting Information Table S4), but the two most overrepresented genes that participate in C4 metabolism, pyruvate orthophosphate dikinase (*PPDK*) and phosphoenol pyruvate carboxylase (*PEPC*), also participate in glycolytic and gluconeogenic reactions making it difficult to distinguish their specific role in C4 metabolism. Polar diatoms still may activate several distinct, interconnected mechanisms to deal with decreased efficiency of CCMs arising from iron and/or light limitation.

In *F. kerguelensis*, the PPP appears to have an important role in meeting the energy demands of the cell, particularly in iron- and/or light-limited cells (Fig. 5; Supporting Information Fig. S4). We observed increased expression of genes involved in the PPP in light-limited cells with threefold overrepresentation under low Fe/low light (−FeLL) (Fig. 5C). The PPP may allow iron-limited cells to bypass the first phase of glycolysis, requiring ATP and reducing equivalents, while producing CO_2 and NADPH. The rate-controlling enzyme of the PPP is a glucose-6-phosphate dehydrogenase (G6PD), the expression of which was overrepresented in all treatments, but to the greatest extent, 10.6-fold, under low Fe (SL) (Fig. 4). Enzymes of the upper phase of glycolysis were weakly overrepresented in all treatments (Fig. 5), with the exception of a fructose-bisphosphate aldolase class I (*FBA*) enzyme. *FBA* class I does not require iron (Smith et al. 2012) and appeared to have an additive effect of iron and light limitation on its gene expression with a 2.9-fold increase ($p = 0.02$) under low Fe (SL), a 4.2-fold increase under low light (+Fe), and a 9.3-fold increase under low Fe/low light (−FeLL) (Fig. 4). On the other hand, FBA class II activity depends on metal catalysis (Marsh and Lebherz 1992) and the gene was weakly expressed in all treatments, although was most abundant under low light (+Fe) (Fig. 3B). *FBA* class II is highly expressed under high iron conditions in laboratory cultures of *Thalassiosira oceanica*, *P. tricornutum*, and *P. granii* (Allen et al. 2012; Lommer et al. 2012; Cohen et al. 2018), but it appears *F. kerguelensis* may rely more on FBA class I under all growth conditions. Enzymes involved in the PPP were also shown to have a key role in the long-term acclimation of *P. tricornutum* to low iron by providing additional reducing equivalents (Nunn et al. 2013), as well as in natural diatom communities in Antarctic waters (Pearson et al. 2015).

Summary

Analysis of the *F. kerguelensis* transcriptome has provided insights into the molecular underpinnings of the

physiological response to iron and light limitation in a polar diatom and identified a subset of genes that could be used as molecular indicators to detect iron and/or light stress in natural assemblages. A dynamic restructuring of carbon and nitrogen metabolisms (i.e., amino acid pathways, sulfur metabolism, and carbon metabolisms) in the low iron/low light condition and a switch to iron-independent genes and isoforms may explain the lack of an additive effect between iron and light on growth rate and photophysiology. However, the overrepresentation of transcripts for genes encoding PR, certain isoforms of flavodoxin and plastocyanin, and FBA class I under the combined low iron and low light treatment, indicate that there was an additive effect between the two resource limitations at the molecular level. At the broader pathway levels, ribosome, sulfur metabolism, and certain amino acid pathways such as BCAAs, AAAs, and cysteine biosynthesis were enhanced in the combined treatment, likely emphasizing the importance of recycling N and C compounds. Newly identified genes that were uniquely responsive to iron limitation and that may play a role in reducing stress include an aquaporin, a peroxiredoxin and a *myo*-inositol dehydrogenase. Diversified photosynthetic isoforms and iron acquisition strategies, along with unique ROS detoxification techniques and metabolic shifts in amino acid recycling and carbon metabolisms may also contribute to the ecological success of this polar diatom in its natural environment.

References

Abelmann, A., R. Gersonde, G. Cortese, G. Kuhn, and V. Smetacek. 2006. Extensive phytoplankton blooms in the Atlantic sector of the glacial Southern Ocean. Paleoceanography **21**: 1–9. doi:10.1029/2005PA001199

Allen, A. E., and others. 2008. Whole-cell response of the pennate diatom *Phaeodactylum tricornutum* to iron starvation. Proc. Natl. Acad. Sci. USA **105**: 10438–10443. doi:10.1073/pnas.0711370105

Allen, A. E., and others. 2011. Evolution and metabolic significance of the urea cycle in photosynthetic diatoms. Nature **473**: 203–207. doi:10.1038/nature10074

Allen, A. E., A. Moustafa, A. Montsant, A. Eckert, P. G. Kroth, and C. Bowler. 2012. Evolution and functional diversification of fructose bisphosphate aldolase genes in photosynthetic marine diatoms. Mol. Biol. Evol. **29**: 367–379. doi:10.1093/molbev/msr223

Arrigo, K. R., A. M. Weiss, and W. O. Smith. 1998. Physical forcing of phytoplankton dynamics in the southwestern Ross Sea. J. Geophys. Res. Oceans **103**: 1007–1021. doi:10.1029/97JC02326

Arrigo, K. R., M. M. Mills, L. R. Kropuenske, G. L. van Dijken, A. C. Alderkamp, and D. H. Robinson. 2010. Photophysiology in two major southern ocean phytoplankton taxa: Photosynthesis and growth of *Phaeocystis antarctica* and *Fragilariopsis cylindrus* under different irradiance levels. Integr. Comp. Biol. **50**: 950–966. doi:10.1093/icb/icq021

Ashworth, J., S. Coesel, A. Lee, E. V. Armbrust, M. V. Orellana, and N. S. Baliga. 2013. Genome-wide diel growth state transitions in the diatom *Thalassiosira pseudonana*. Proc. Natl. Acad. Sci. USA **110**: 7518–7523. doi:10.1073/pnas.1300962110

Assmy, P., J. Henjes, V. Smetacek, and M. Montresor. 2006. Auxospore formation by the silica-sinking, oceanic diatom *Fragilariopsis kerguelensis* (Bacillariophyceae). J. Phycol. **42**: 1002–1006. doi:10.1111/j.1529-8817.2006.00260.x

Assmy, P., and others. 2013. Thick-shelled, grazer-protected diatoms decouple ocean carbon and silicon cycles in the iron-limited Antarctic Circumpolar Current. Proc. Natl. Acad. Sci. USA. **110**(51):20633–20638. doi:10.1073/pnas.1309345110

Bailleul, B., A. Rogato, A. de Martino, S. Coesel, P. Cardol, C. Bowler, A. Falciatore, and G. Finazzi. 2010. An atypical member of the light-harvesting complex stress-related protein family modulates diatom responses to light. Proc. Natl. Acad. Sci. USA **107**: 18214–18219. doi:10.1073/pnas.1007703107

Bailleul, B., and others. 2015. Energetic coupling between plastids and mitochondria drives CO_2 assimilation in diatoms. Nature **524**: 366–369. doi:10.1038/nature14599

Bender, S. J., C. A. Durkin, C. T. Berthiaume, R. L. Morales, and E. V. Armbrust. 2014. Transcriptional responses of three model diatoms to nitrate limitation of growth. Front. Mar. Sci. **1**: 1–15. doi:10.3389/fmars.2014.00003

Berlett, B. S., and E. R. Stadtman. 1997. Protein oxidation in aging, disease, and oxidative stress. J. Biol. Chem. **272**: 20313–20316. doi:10.1074/jbc.272.33.20313

Bertrand, E. M., A. E. Allen, C. L. Dupont, T. M. Norden-Krichmar, J. Bai, R. E. Valas, and M. A. Saito. 2012. Influence of cobalamin scarcity on diatom molecular physiology and identification of a cobalamin acquisition protein. Proc. Natl. Acad. Sci. USA **109**: 1762–1771. doi:10.1073/pnas.1201731109

Bertrand, E. M., and others. 2015. Phytoplankton–bacterial interactions mediate micronutrient colimitation at the coastal Antarctic sea ice edge. Proc. Natl. Acad. Sci. USA **112**: 9938–9943. doi:10.1073/pnas.1501615112

Blain, S., and others. 2007. Effect of natural iron fertilization on carbon sequestration in the Southern Ocean. Nature **446**: 1070–1074. doi:10.1038/nature05700

Boyd, P. W. 2002. Environmental factors controlling phytoplankton processes in the Southern Ocean. J. Phycol. **38**: 844–861. doi:10.1046/j.1529-8817.2002.t01-1-01203.x

Boyd, P. W., and others. 2000. A mesoscale phytoplankton bloom in the polar Southern Ocean stimulated by iron fertilization. Nature **407**: 695–702. doi:10.1038/35037500

Boyd, P. W., A. C. Crossley, G. R. DiTullio, F. B. Griffiths, D. A. Hutchins, B. Queguiner, P. N. Sedwick, and T. W. Trull. 2001. Control of phytoplankton growth by iron supply and irradiance in the subantarctic Southern Ocean: Experimental results from the SAZ Project. J. Geophys. Res. **106**: 31573–31583. doi:10.1029/2000JC000348

Boyd, P. W., and others. 2007. Mesoscale iron enrichment experiments 1993–2005: Synthesis and future directions. Science **315**: 612–617. doi:10.1126/science.1131669

Boyd, P. W., and others. 2015. Physiological responses of a Southern Ocean diatom to complex future ocean conditions. Nat. Clim. Chang. **6**: 207–213. doi:10.1038/nclimate2811

Brand, L. E., R. L. Guillard, and L. S. Murphy. 1981. A method for the rapid and precise determination of acclimated phytoplankton reproductions rates. J. Plankton Res. **3**: 193–201. doi:10.1016/0022-0981(86)90205-4

Bromke, M. A. 2013. Amino acid biosynthesis pathways in diatoms. Metabolites **3**: 294–311. doi:10.3390/metabo3020294

Cassar, N., M. L. Bender, B. A. Barnett, S. Fan, W. J. Moxim, H. Levy, and B. Tilbrook. 2007. The Southern Ocean biological response to aeolian iron deposition. Science **317**: 1067–1070. doi:10.1126/science.1144602

Cassar, N., and others. 2011. The influence of iron and light on net community production in the Subantarctic and Polar Frontal Zones. Biogeosciences **8**: 227–237. doi:10.5194/bg-8-227-2011

Chappell, P. D., L. P. Whitney, J. R. Wallace, A. I. Darer, S. Jean-Charles, and B. D. Jenkins. 2014. Genetic indicators of iron limitation in wild populations of *Thalassiosira oceanica* from the northeast Pacific Ocean. ISME J. **9**: 1–11. doi:10.1038/ismej.2014.171

Cohen, N. R., K. A. Ellis, W. G. Burns, R. H. Lampe, N. Schuback, Z. Johnson, S. Sañudo-Wilhelmy, and A. Marchetti. 2017*a*. Iron and vitamin interactions in marine diatom isolates and natural assemblages of the Northeast Pacific Ocean. Limnol. Oceanogr. **62**: 2076–2096. doi:10.1002/lno.10552

Cohen, N. R., and others. 2017*b*. Diatom transcriptional and physiological responses to changes in iron bioavailability across ocean provinces. Front. Mar. Sci. **4**: 360. doi:10.3389/fmars.2017.00360

Cohen, N. R., W. Gong, D. M. Moran, M. R. McIlvin, M. A. Saito, and A. Marchetti. 2018. Transcriptomic and proteomic responses of the oceanic diatom *Pseudo-nitzschia granii* to iron limitation. Environ. Microbiol. **20**: 3109–3126. doi:10.1111/1462-2920.14386

Davis, A., R. Abbriano, S. R. Smith, and M. Hildebrand. 2016. Clarification of photorespiratory processes and the role of malic enzyme in diatoms. Protist **168**: 134–153. doi:10.1016/j.protis.2016.10.005

de Baar, H. J., A. G. Buma, R. F. Nolting, G. C. Cadee, G. Jacques, and P. J. Tréguer. 1990. On iron limitation of the Southern Ocean: Experimental observations in the Weddell and Scotia Seas. Mar. Ecol. Prog. Ser. **65**: 105–122. doi:10.3354/meps065105

Edwards, R., and P. Sedwick. 2001. Iron in East Antarctic snow: Implications for atmospheric iron deposition and algal production in Antarctic waters. Geophys. Res. Lett. **28**: 3907–3910. doi:10.1029/2001GL012867

Feng, Y., and others. 2010. Interactive effects of iron, irradiance and CO_2 on Ross Sea phytoplankton. Deep-Sea Res. Part I Oceanogr. Res. Pap. **57**: 368–383. doi:10.1016/j.dsr.2009.10.013

Fortunato, A. E., and others. 2016. Diatom phytochromes reveal the existence of far-red-light-based sensing in the ocean. Plant Cell **28**: 616–628. doi:10.1105/tpc.15.00928

Galbraith, E. D., A. Gnanadesikan, J. P. Dunne, and M. R. Hiscock. 2010. Regional impacts of iron-light colimitation in a global biogeochemical model. Biogeosciences **7**: 1043–1064. doi:10.5194/bg-7-1043-2010

Giordano, M., A. Norici, and R. Hell. 2005. Sulfur and phytoplankton: Acquisition, metabolism and impact on the environment. New Phytol. **166**: 371–382. doi:10.1111/j.1469-8137.2005.01335.x

Gorbunov, M. Y., and P. G. Falkowski. 2005. Fluorescence induction and relaxation (FIRe) technique and instrumentation for monitoring photosynthetic processes and primary production in aquatic ecosystems, p. 1029–1031. *In* A. van der Est and D. Bruce [eds.], Photosynthesis: Fundamental aspects to global perspectives. Allen Press.

Gross, W., and A. Meyer. 2003. Distribution of *myo*-inositol dehydrogenase in algae. Eur. J. Phycol. **38**: 191–194. doi:10.1080/1364253031000121705

Groussman, R. D., M. S. Parker, and E. V. Armbrust. 2015. Diversity and evolutionary history of iron metabolism genes in diatoms. PLoS One **10**: e0129081. doi:10.1371/journal.pone.0129081

Gruber, N., and others. 2009. Oceanic sources, sinks, and transport of atmospheric CO_2. Global Biogeochem. Cycles **23**: GB1005 doi:10.1029/2008GB003349

Haimovich-Dayan, M., N. Garfinkel, D. Ewe, Y. Marcus, A. Gruber, H. Wagner, P. G. Kroth, and A. Kaplan. 2013. The role of C4 metabolism in the marine diatom *Phaeodactylum tricornutum*. New Phytol. **197**: 177–185. doi:10.1111/j.1469-8137.2012.04375.x

Hamilton, N. 2018. ggtern: An extension to 'ggplot2', for the creation of ternary diagrams. R package version 2.2.2. Available from https://CRAN.R-project.org/package=ggtern. Accessed September 2018.

Hamm, C. E., R. Merkel, O. Springer, P. Jurkojc, C. Maiert, K. Prechtelt, and V. Smetacek. 2003. Architecture and material properties of diatom shells provide effective mechanical protection. Nature **421**: 841–843. doi:10.1038/nature01416

Hildebrandt, T. M., A. Nunes Nesi, W. L. Araújo, and H. P. Braun. 2015. Amino acid catabolism in plants. Mol. Plant **8**: 1563–1579. doi:10.1016/j.molp.2015.09.005

Hockin, N. L., T. Mock, F. Mulholland, S. Kopriva, and G. Malin. 2012. The response of diatom central carbon metabolism to nitrogen starvation is different from that of green algae and higher plants. Plant Physiol. **158**: 299–312. doi:10.1104/pp.111.184333

Hoffmann, L. J., I. Peeken, and K. Lochte. 2007. Effects of iron on the elemental stoichiometry during EIFEX and in the

diatoms *Fragilariopsis kerguelensis* and *Chaetoceros dichaeta*. Biogeosciences **4**: 569–579. doi:10.5194/bg-4-569-2007

Hoppe, C. J. M., C. S. Hassler, C. D. Payne, P. D. Tortell, and S. Trimborn. 2013. Iron limitation modulates ocean acidification effects on Southern Ocean phytoplankton communities. PLoS One **8**(11): e79890. doi:10.1371/journal.pone.0079890

Imlay, J. A. 2008. Cellular defenses against superoxide and hydrogen peroxide. Annu. Rev. Biochem. **77**: 755–776. doi:10.1146/annurev.biochem.77.061606.161055

Iseli, C., C. V. Jongeneel, and P. Bucher. 1999. ESTScan: A program for detecting, evaluating, and reconstructing potential coding regions in EST sequences. Proc. Int. Conf. Intell. Syst. Mol. Biol. **99**: 138–148.

Jeanjean, R., A. Latifi, H. C. P. Matthijs, and M. Havaux. 2008. The PsaE subunit of photosystem I prevents light-induced formation of reduced oxygen species in the cyanobacterium *Synechocystis* sp. PCC 6803. Biochim. Biophys. Acta **1777**: 308–316. doi:10.1016/j.bbabio.2007.11.009

Kanehisa, M., and others. 2006. From genomics to chemical genomics: New developments in KEGG. Nucleic Acids Res. **34**: D354–D357. doi:10.1093/nar/gkj102

Kazamia, E., and others. 2018. Endocytosis-mediated siderophore uptake as a strategy for Fe acquisition in diatoms. Sci. Adv. **4**: 1–14. doi:10.1126/sciadv.aar4536

Keeling, P. J., and others. 2014. The Marine Microbial Eukaryote Transcriptome Sequencing Project (MMETSP): Illuminating the functional diversity of eukaryotic life in the oceans through transcriptome sequencing. PLoS Biol. **12**: e1001889. doi:10.1371/journal.pbio.1001889

Kloer, D. P., S. Ruch, S. Al-Babili, P. Beyer, and G. E. Schulz. 2005. The structure of a retinal-forming carotenoid oxygenase. Science **308**: 267–269. doi:10.1126/science.1108965

Koch, F., S. Beszteri, L. Harms, and S. Trimborn. 2019. The impacts of iron limitation and ocean acidification on the cellular stoichiometry, photophysiology, and transcriptome of *Phaeocystis antarctica*. Limnol. Oceanogr. **64**: 357–375. doi:10.1002/lno.11045

Koid, A. E., Z. Liu, R. Terrado, A. C. Jones, D. A. Caron, and K. B. Heidelberg. 2014. Comparative transcriptome analysis of four prymnesiophyte algae. PLoS One **9**: e97801. doi:10.1371/journal.pone.0097801

Kroth, P. G., and others. 2008. A model for carbohydrate metabolism in the diatom *Phaeodactylum tricornutum* deduced from comparative whole genome analysis. PLoS One **3**(1):e1426. doi:10.1371/journal.pone.0001426

Kustka, A. B., A. E. Allen, and F. M. M. Morel. 2007. Sequence analysis and transcriptional regulation of iron acquisition genes in two marine diatoms. J. Phycol. **43**: 715–729. doi:10.1111/j.1529-8817.2007.00359.x

La Roche, J., P. W. Boyd, R. M. L. McKay, and R. J. Geider. 1996. Flavodoxin as an *in situ* marker for iron stress in phytoplankton. Nature **382**: 802–805. doi:10.1038/382802a0

Lamkemeyer, P., and others. 2006. Peroxiredoxin Q of *Arabidopsis thaliana* is attached to the thylakoids and functions in context of photosynthesis. Plant J. **45**: 968–981. doi:10.1111/j.1365-313X.2006.02665.x

Langmead, B., and S. L. Salzberg. 2012. Fast gapped-read alignment with Bowtie 2. Nat. Methods **9**: 357–359. doi:10.1038/nmeth.1923

Laxa, M., J. König, K. J. Dietz, and A. Kandlbinder. 2007. Role of the cysteine residues in *Arabidopsis thaliana* cyclophilin CYP20-3 in peptidyl-prolyl cis-trans isomerase and redox-related functions. Biochem. J. **401**: 287–297. doi:10.1042/BJ20061092

Li, W., and A. Godzik. 2006. Cd-hit: A fast program for clustering and comparing large sets of protein or nucleotide sequences. Bioinformatics **22**: 1658–1659. doi:10.1093/bioinformatics/btl158

Lima, M. S., and D. R. Smith. 2017. Pervasive transcription of mitochondrial, plastid, and nucleomorph genomes across diverse plastid-bearing species. Genome Biol. Evol. **9**: 2650–2657. doi:10.1093/gbe/evx207

Llewellyn, C. A., and R. L. Airs. 2010. Distribution and abundance of MAAs in 33 species of microalgae across 13 classes. Mar. Drugs **8**: 1273–1291. doi:10.3390/md8041273

Lommer, M., and others. 2012. Genome and low-iron response of an oceanic diatom adapted to chronic iron limitation. Genome Biol. **13**: R66. doi:10.1186/gb-2012-13-7-r66

Lottaz, C., C. Iseli, C. V. Jongeneel, and P. Bucher. 2003. Modeling sequencing errors by combining hidden Markov models. Bioinformatics **19**: ii103–ii112. doi:10.1093/bioinformatics/btg1067

Luo, R., and others. 2015. SOAPdenovo2: An empirically improved memory-efficient short-read *de novo* assembler. Gigascience **4**: 1. doi:10.1186/s13742-015-0069-2

Maldonado, M. T., A. E. Allen, J. S. Chong, K. Lin, D. Leus, N. Karpenko, and S. L. Harris. 2006. Copper-dependent iron transport in coastal and oceanic diatoms. Limnol. Oceanogr. **51**: 1729–1743. doi:10.4319/lo.2006.51.4.1729

Marchetti, A., M. T. Maldonado, E. S. Lane, and P. J. Harrison. 2006. Iron requirements of the pennate diatom *Pseudo-nitzschia*: Comparison of oceanic (high-nitrate, low-chlorophyll waters) and coastal species. Limnol. Oceanogr. **51**: 2092–2101. doi:10.4319/lo.2006.51.5.2092

Marchetti, A., and N. Cassar. 2009. Diatom elemental and morphological changes in response to iron limitation: A brief review with potential paleoceanographic applications. Geobiology **7**: 419–431. doi:10.1111/j.1472-4669.2009.00207.x

Marchetti, A., and others. 2009. Ferritin is used for iron storage in bloom-forming marine pennate diatoms. Nature **457**: 467–470. doi:10.1038/nature07539

Marchetti, A., and others. 2012. Comparative metatranscriptomics identifies molecular bases for the physiological responses of phytoplankton to varying iron availability. Proc. Natl. Acad. Sci. USA **109**: E317–E325. doi:10.1073/pnas.1118408109

Marchetti, A., D. Catlett, B. M. Hopkinson, K. Ellis, and N. Cassar. 2015. Marine diatom proteorhodopsins and their potential role in coping with low iron availability. ISME J. **9**: 1–4. doi:10.1038/ismej.2015.74

Marchetti, A., and M. Maldonado. 2016. Iron, p. 233–280. *In* M. A. Borowitzka, J. Beardall, and J. A. Raven [eds.], The physiology of microalgae. Springer.

Marchetti, A., C. M. Moreno, N. H. Cohen, I. Oleinikov, K. deLong, B. S. Twining, E. V. Armbrust, and R. H. Lampe. 2017. Development of a molecular-based index for assessing iron status in bloom-forming pennate diatoms. J. Phycol. **53**: 820–832. doi:10.1111/jpy.12539

Marsh, J. J., and H. G. Lebherz. 1992. Fructose-bisphosphate aldolases—an evolutionary history. Trends Biochem. Sci. **17**: 110–113. doi:10.1016/0968-0004(92)90247-7

Martin, J. H. 1990. Glacial-interglacial CO_2 change: The iron hypothesis. Paleoceanography **5**: 1–13. doi:10.1029/PA005i001p00001

Matsuda, Y., B. M. Hopkinson, K. Nakajima, C. L. Dupont, and Y. Tsuji. 2017. Mechanisms of carbon dioxide acquisition and CO_2 sensing in marine diatoms: A gateway to carbon metabolism. Philos. Trans. R. Soc. B Biol. Sci. **372**: 20160403. doi:10.1098/rstb.2016.0403

McQuaid, J. B., and others. 2018. Carbonate-sensitive phytotransferrin controls high-affinity iron uptake in diatoms. Nature **555**: 534–537. doi:10.1038/nature25982

Meyer, E., G. V. Aglyamova, and M. V. Matz. 2011. Profiling gene expression responses of coral larvae (*Acropora millepora*) to elevated temperature and settlement inducers using a novel RNA-Seq procedure. Mol. Ecol. **20**: 3599–3616. doi:10.1111/j.1365-294X.2011.05205.x

Mitchell, B. G., E. A. Brody, O. Holm-Hansen, C. Mcclain, and L. Doherty. 1991. Light limitation of phytoplankton biomass and macronutrient utilization in the Southern Ocean. Limnol. Oceanogr. **36**: 1662–1667. doi:10.4319/lo.1991.36.8.1662

Mock, T., and others. 2017. Evolutionary genomics of the cold-adapted diatom *Fragilariopsis cylindrus*. Nature **541**: 536–540. doi:10.1038/nature20803

Moreno, C. M., Y. Lin, S. Davies, E. Monbureau, N. Cassar, and A. Marchetti. 2018. Examination of gene repertoires and physiological responses to iron and light limitation in Southern Ocean diatoms. Polar Biol. **41**: 679–696. doi:10.1007/s00300-017-2228-7

Morrissey, J., and others. 2015. A novel protein, ubiquitous in marine phytoplankton, concentrates iron at the cell surface and facilitates uptake. Curr. Biol. **25**: 364–371. doi:10.1016/j.cub.2014.12.004

Moseley, J. L., T. Allinger, S. Herzog, P. Hoerth, E. Wehinger, S. Merchant, and M. Hippler. 2002. Adaptation to Fe-deficiency requires remodeling of the photosynthetic apparatus. EMBO J. **21**: 6709–6720. doi:10.1093/emboj/cdf666

Nakajima, K., A. Tanaka, and Y. Matsuda. 2013. SLC4 family transporters in a marine diatom directly pump bicarbonate from seawater. Proc. Natl. Acad. Sci. USA **110**: 1767–1772. doi:10.1073/pnas.1216234110

Nuester, J., S. Vogt, and B. S. Twining. 2012. Localization of iron within centric diatoms of the genus *Thalassiosira*. J. Phycol. **48**: 626–634. doi:10.1111/j.1529-8817.2012.01165.x

Nunn, B. L., J. F. Faux, A. A. Hippmann, M. T. Maldonado, H. R. Harvey, D. R. Goodlett, P. W. Boyd, and R. F. Strzepek. 2013. Diatom proteomics reveals unique acclimation strategies to mitigate Fe limitation. PLoS One **8**: e75653. doi:10.1371/journal.pone.0075653

Pearson, G. A., and others. 2015. Metatranscriptomes reveal functional variation in diatom communities from the Antarctic Peninsula. Isme J. **9**: 2275–2289. doi:10.1038/ismej.2015.40

Peers, G., and N. M. Price. 2004. A role for manganese in superoxide dismutases and growth of iron-deficient diatoms. Limnol. Oceanogr. **49**: 1774–1783. doi:10.4319/lo.2004.49.5.1774

Peers, G., and N. M. Price. 2006. Copper-containing plastocyanin used for electron transport by an oceanic diatom. Nature **441**: 341–344. doi:10.1038/nature04630

Peters, E., and D. N. Thomas. 1996. Prolonged darkness and diatom mortality I: Marine antarctic species. J. Exp. Mar. Biol. Ecol. **207**: 25–41. doi:10.1016/S0022-0981(96)02520-8

Pfaffl, M. W. 2001. A new mathematical model for relative quantification in real-time RT–PCR. Nucleic Acids Res. **29**: e45. doi:10.1093/nar/29.9.e45

Portune, K. J., C. R. Voolstra, M. Medina, and A. M. Szmant. 2010. Development and heat stress-induced transcriptomic changes during embryogenesis of the scleractinian coral *Acropora palmata*. Mar. Genomics **3**: 51–62. doi:10.1016/j.margen.2010.03.002

Price, N. M., G. I. Harrison, J. G. Hering, P. M. V. Nirel, B. Palenik, and F. M. M. Morel. 1989. Preparation and chemistry of the artificial algal culture medium Aquil. Biol. Oceanogr. **6**: 443–461. doi:10.1080/01965581.1988.10749544

Raven, J. A. 2013. Iron acquisition and allocation in stramenopile algae. J. Exp. Bot. **64**: 2119–2127. doi:10.1093/jxb/ert121

Reinfelder, J. R. 2011. Carbon concentrating mechanisms in eukaryotic marine phytoplankton. Ann. Rev. Mar. Sci. **3**: 291–315. doi:10.1146/annurev-marine-120709-142720

Robinson, M. D., and G. K. Smyth. 2007. Small-sample estimation of negative binomial dispersion, with applications to SAGE data. Biostatistics **9**: 321–332. doi:10.1093/biostatistics/kxm030

Robinson, M. D., D. J. McCarthy, and G. K. Smyth. 2009. edgeR: A bioconductor package for differential expression analysis of digital gene expression data. Bioinformatics **26**: 139–140. doi:10.1093/bioinformatics/btp616

Rokitta, S. D., P. Von Dassow, B. Rost, and U. John. 2014. *Emiliania huxleyi* endures N-limitation with an efficient metabolic budgeting and effective ATP synthesis. BMC Genomics **15**: 1–14. doi:10.1186/1471-2164-15-1051

Saba, G. K., and others. 2014. Winter and spring controls on the summer food web of the coastal West Antarctic Peninsula. Nat. Commun. **5**: 4318. doi:10.1038/ncomms5318

Sallée, J. B., K. G. Speer, and S. R. Rintoul. 2010. Zonally asymmetric response of the Southern Ocean mixed-layer depth to the Southern Annular Mode. Nat. Geosci. **3**: 273–279. doi:10.1038/ngeo812

Sarmiento, J. L., N. Gruber, M. A. Brzezinski, and J. P. Dunne. 2004. High-latitude controls of thermocline nutrients and low latitude biological productivity. Nature **427**: 56–60. doi:10.1038/nature02127

Simão, F. A., R. M. Waterhouse, P. Ioannidis, E. V. Kriventseva, and E. M. Zdobnov. 2015. BUSCO: Assessing genome assembly and annotation completeness with single-copy orthologs. Bioinformatics **31**: 3210–3212. doi:10.1093/bioinformatics/btv351

Simpson, J. T., K. Wong, S. D. Jackman, J. E. Schein, S. J. M. Jones, and I. Birol. 2009. ABySS: A parallel assembler for short read sequence data. Genome Res. **19**: 1117–1123. doi:10.1101/gr.089532.108

Simpson, J. T., and R. Durbin. 2011. Efficient *de novo* assembly of large genomes using compressed data structures. Genome Res. **22**: 549–556. doi:10.1101/gr.126953.111

Smith, S. R., R. M. Abbriano, and M. Hildebrand. 2012. Comparative analysis of diatom genomes reveals substantial differences in the organization of carbon partitioning pathways. Algal Res. **1**: 2–16. doi:10.1016/j.algal.2012.04.003

Smith, S. R., J. T. F. Gillard, A. B. Kustka, J. P. McCrow, J. H. Badger, H. Zheng, and A. M. New. 2016. Transcriptional orchestration of the global cellular response of a model pennate diatom to diel light cycling under iron limitation. PLoS Genet. **12**: e1006490. doi:10.1371/journal.pgen.1006490

Strauss, J. 2012. A genomic analysis using RNA-Seq to investigate the adaptation of the psychrophilic diatom *Fragilariopsis cylindrus* to the polar environment. Ph.D. thesis. Univ. of East Anglia.

Strzepek, R. F., and P. J. Harrison. 2004. Photosynthetic architecture differs in coastal and oceanic diatoms. Nature **431**: 689–692. doi:10.1038/nature02954

Strzepek, R. F., M. T. Maldonado, K. A. Hunter, R. D. Frew, and P. W. Boyd. 2011. Adaptive strategies by Southern Ocean phytoplankton to lessen iron limitation: Uptake of organically complexed iron and reduced cellular iron requirements. Limnol. Oceanogr. **56**: 1983–2002. doi:10.4319/lo.2011.56.6.1983

Strzepek, R. F., K. A. Hunter, R. D. Frew, P. J. Harrison, and P. W. Boyd. 2012. Iron-light interactions differ in Southern Ocean phytoplankton. Limnol. Oceanogr. **57**: 1182–1200. doi:10.4319/lo.2012.57.4.1182

Strzepek, R. F., P. W. Boyd, and W. G. Sunda. 2019. Photosynthetic adaptation to low iron, light, and temperature in Southern Ocean phytoplankton. Proc. Natl. Acad. Sci. USA **116**: 4388–4393. doi:10.1073/pnas.1810886116

Suggett, D. J., C. M. Moore, A. E. Hickman, and R. J. Geider. 2009. Interpretation of fast repetition rate (FRR) fluorescence: Signatures of phytoplankton community structure versus physiological state. Mar. Ecol. Prog. Ser. **376**: 1–19. doi:10.3354/meps07830

Sunda, W. G., and S. A. Huntsman. 1995. Iron uptake and growth limitation in oceanic and coastal phytoplankton. Mar. Chem. **50**: 189–206. doi:10.1016/0304-4203(95)00035-P

Timmermans, K. R., L. J. A. Gerringa, H. J. W. de Baar, B. van der Wagt, M. J. W. Veldhuis, J. T. M. de Jong, P. L. Croot, and M. Boye. 2001. Growth rates of large and small Southern Ocean diatoms in relation to availability of iron in natural seawater. Limnol. Oceanogr. **46**: 260–266. doi:10.4319/lo.2001.46.2.0260

Timmermans, K. R., B. Van Der Wagt, and H. J. W. de Baar. 2004. Growth rates, half saturation constants, and silicate, nitrate, and phosphate depletion in relation to iron availability of four large open-ocean diatoms from the Southern Ocean. Limnol. Oceanogr. **49**: 2141–2151. doi:10.4319/lo.2004.49.6.2141

Timmermans, K. R., and B. van der Wagt. 2010. Variability in cell size, nutrient depletion, and growth rates of the southern ocean diatom *Fragilariopsis kerguelensis* (bacillariophyceae) after prolonged iron limitation. J. Phycol. **46**: 497–506. doi:10.1111/j.1529-8817.2010.00827.x

Tréguer, P., D. M. Nelson, A. J. Van Bennekom, D. J. Demaster, A. Leynaert, and B. Quéguiner. 1995. The silica balance in the world ocean: A reestimate. Science **268**: 375–379. doi:10.1126/science.268.5209.375

Tréguer, P., D. M. Nelson, A. J. Van Bennekom, D. J. Demaster, B. Quéguiner, P. Tréguer, A. Leynaert, and B. Queguiner. 2014. The silica balance in the world ocean: A reestimate. Science **268**: 375–379.

Valluru, R., and W. Van den Ende. 2011. *Myo*-inositol and beyond - emerging networks under stress. Plant Sci. **181**: 387–400. doi:10.1016/j.plantsci.2011.07.009

van Oijen, T. 2004. Light rather than iron controls photosynthate production and allocation in Southern Ocean phytoplankton populations during austral autumn. J. Plankton Res. **26**: 885–900. doi:10.1093/plankt/fbh088

Vavilin, D. V., S. Y. Ermakova-Gerdes, A. T. Keilty, and W. F. J. Vermaas. 1999. Tryptophan at position 181 of the D2 protein of photosystem II confers quenching of variable fluorescence of chlorophyll: Implications for the mechanism of energy-dependent quenching. Biochemistry **38**: 14690–14696. doi:10.1021/bi9915622

Veluchamy, A., and others. 2013. Insights into the role of DNA methylation in diatoms by genome-wide profiling in *Phaeodactylum tricornutum*. Nat. Commun. **4**: 2091 doi:10.1038/ncomms3091

Wickham, H. 2016. ggplot2: Elegant graphics for data analysis. Springer Verlag.

Xiaoqui, H., and M. Anup. 1999. CAP3: A DNA sequence assembly program. Genome Res. **9**: 868–877.

Zielinski, U., and R. Gersonde. 1997. Diatom distribution in Southern Ocean surface sediments (Atlantic sector): Implications for paleoenvironmental reconstructions. Palaeogeogr. Palaeoclimatol. Palaeoecol. **129**: 213–250. doi:10.1016/S0031-0182(96)00130-7

Acknowledgments

We thank Phillip Assmy for providing the strain of *F. kerguelensis* used in this study, Olivia Torano for coding assistance, and Barbara MacGregor for providing valuable feedback on the manuscript. Funding for sequencing was provided by the Moore Foundation, and transcriptome assembly was performed at the National Center for Genome Resources. This research was supported by grants from NSF OPP1341479 and OPP1745036 grants (to A.M.). C.M.M. was partially supported by a Gates Millennium Fellowship. We are thankful for the careful review and suggestions for improving the manuscript from two anonymous reviewers.

Conflict of Interest

None declared.

Submitted 29 March 2019
Revised 24 September 2019
Accepted 11 December 2019

Associate editor: Heidi Sosik